

The Canonical Function Method and its applications in Quantum Physics

C. Tannous[†], K. Fakhreddine^{*} and J. Langlois[§]

[†]Laboratoire de Magnétisme de Bretagne, CNRS-FRE 2697,

[§]Laboratoire des Collisions Electroniques et Atomiques,
Université de Bretagne Occidentale, BP: 809 Brest CEDEX, 29285 France

^{*}Faculty of Science, Lebanese University and CNRS, P.O. Box: 113-6546, Beirut, Lebanon

The Canonical Function Method (CFM) is a powerful method that solves the radial Schrödinger equation for the eigenvalues directly without having to evaluate the eigenfunctions. It is applied to various quantum mechanical problems in Atomic and Molecular physics with presence of regular or singular potentials. It has also been developed to handle single and multiple channel scattering problems where the phaseshift is required for the evaluation of the scattering cross-section. Its controllable accuracy makes it a valuable tool for the evaluation of vibrational levels of cold molecules, a sensitive test of Bohr correspondence principle and a powerful method to tackle local and non-local spin dependent problems. *To submit to Rev. Mod. Phys. (2006).*

Contents

I. Introduction	1
II. The Canonical Function Method (CFM)	2
A. The Multichannel case	4
B. Evaluation of energy spectra and phaseshift	6
III. Potential estimation from spectroscopy	7
A. Optimisation procedure	7
IV. Vibrational spectra of Cold Molecules	8
A. Vibrational energy levels of the $^{23}\text{Na}_2$ molecule	9
B. Lennard-Jones molecules	13
V. Test of Bohr Correspondance Principle	14
A. Semi-classical analysis	14
B. Test with the $^{23}\text{Na}_2$ molecule	16
C. Test with Lennard-Jones molecules	17
VI. Exchange: local and non-local	17
A. The integro-differential equation	18
B. The CFM for solving the DWPO equations	20
C. Phaseshift calculation	21
D. Phaseshift accuracy and comparison to the S-IEM	22
VII. One-dimensional potential problems	25
VIII. Conclusions	26
References	29

I. INTRODUCTION

The Canonical Function Method (CFM) is a powerful means for solving the Radial Schrödinger Equation (RSE), a singular boundary value problem (SBVP) with a stringent dual requirement of regularity near the origin ($r \sim 0$) where the potential is large and near infinity ($r \rightarrow \infty$) where the potential is very small.

The CFM turns this SBVP into a regular initial value problem and allows full and accurate determination of the spectrum of the Schrödinger operator.

The CFM can handle bound states and scattering states, spinless and spin-dependent, single channel or multi-channel problems and possesses several features

that makes it of interest for solving a large variety of problems in Quantum Mechanics of Atoms, Molecules and Scattering. Those capabilities are based essentially on the following main characteristics:

- Its capability to transform a SVBP into a regular initial value problem (RIVP), means mathematically that the CFM belongs to a family of Invariant Embedding Methods (IEM). Those essentially transform a boundary value problem into an initial value problem. The CFM is even more powerful than standard IEM techniques since it turns the nature of the problem from singular to regular.
- The evaluation of the Schrödinger operator spectrum is done without performing diagonalization, bypassing the evaluation of the eigenfunctions. This allows to preserve a high degree of numerical precision that is required in solving sensitive eigenvalue problems arising in Cold Molecules or large n -limit problems where levels to evaluate are very close to the continuum limit or dissociation.

The numerical precision gained with the bypass of intermediate diagonalization operations is reminiscent of the Golub-Reinsch algorithm (see for instance ref. (50)) used for the singular value decomposition of arbitrary rectangular matrices.

This review is organised as follows: The next section is a description of the CFM with highlights of its mathematical aspects and its generalisation to the multichannel case. In section III the mathematical and numerical techniques of the radial Schrödinger equation are discussed and the full procedure for dealing with general potentials, energy levels and evaluation of phaseshifts is detailed in section IV. In the rest of the sections, we apply the CFM method systematically to a variety of problems highlighting its successes and showing its limitations whenever they show up. While, the versatility of the method is illustrated with the help of this selection of examples, the list below is by no means exhaustive but serves the purpose of underlining the breadth of applications of the CFM.

- Energy levels for regular and singular potentials (radial case)
- Potential estimation (in parametric or pseudo form) from spectroscopic data
- Test of the Bohr Correspondence Principle
- Vibrational energy levels of Cold Molecules and application to the $^{23}\text{Na}_2$ molecule in the 0_g^- and 1_u electronic states. The Lennard-Jones molecule case is also studied.
- Local and Non-Local Exchange problems.
- Accurate Phase shift evaluation for regular and singular potentials.

In the last section before the conclusion, we treat the general but non obvious (regular and singular) 1D potentials to illustrate how the method can be applied in this case of lesser interest than the 3D's.

In the Appendix we provide information linking the various units used since the review contains results spanning several fields of physics where different systems of units are used. The boundary conditions affecting the spectrum determination via the matching conditions at a single radial point are also discussed in the Appendix.

II. THE CANONICAL FUNCTION METHOD (CFM)

The CFM (29) is a powerful means for solving the Radial Schrödinger Equation (RSE). The mathematical difficulty of the RSE lies in the fact it is a singular boundary value problem. The CFM turns it into a regular initial value problem and allows the full determination of the spectrum of the Schrödinger operator bypassing the evaluation of the eigenfunctions.

The partial wave form of the RSE is written as:

$$-\frac{\hbar^2}{2\mu} \frac{d^2 u_l(E; r)}{dr^2} + \left[V(r) + \frac{\hbar^2}{2\mu} \frac{l(l+1)}{r^2} \right] u_l(E; r) = E u_l(E; r) \quad (1)$$

where μ is the reduced mass and $u_l(E; r)$ is the reduced probability amplitude for orbital angular momentum l and eigenvalue E .

The boundary conditions are:

$$\lim_{r \rightarrow 0} u_l(r) = 0; \quad \lim_{r \rightarrow +\infty} u_l(r) = 0 \quad (2)$$

The CFM developed initially by Kobeissi (35) and his coworkers to integrate the RSE, consists of writing the general solution $y(r)$ representing the probability amplitude $u_l(E; r)$ as a function of the radial distance r in terms of two basis functions $\alpha(E; r)$ and $\beta(E; r)$ for some energy E .

Generally, the RSE is rewritten in a system of units such that $\hbar = 1, 2\mu = 1$ (see Appendix on units):

$$\frac{d^2 y(r)}{dr^2} = \left[V(r) + \frac{l(l+1)}{r^2} - E \right] y(r) \quad (3)$$

At a selected distance r_0 , a well defined set of initial conditions are satisfied by the canonical functions and their derivatives ie: $\alpha(E; r_0) = 1$ with $\alpha'(E; r_0) = 0$ and $\beta(E; r_0) = 0$ with $\beta'(E; r_0) = 1$. Thus we write:

$$y(r) = y(r_0)\alpha(E; r) + y'(r_0)\beta(E; r) \quad (4)$$

The method of solving the RSE is to proceed from r_0 simultaneously towards the origin ($r \rightarrow 0$) and towards infinity ($r \rightarrow \infty$). Expressing the continuity condition of the "wavefunction" $y(r)$ and its derivative $y'(r)$ at the point r_0 from the left ($r \rightarrow 0$) and right ($r \rightarrow \infty$) yields (see Appendix on matching and boundary conditions):

$$\begin{aligned} \left. \frac{y'(r_0)}{y(r_0)} \right]_- &= -\frac{\alpha(E; 0)}{\beta(E; 0)} \\ \left. \frac{y'(r_0)}{y(r_0)} \right]_+ &= -\frac{\alpha(E; \infty)}{\beta(E; \infty)} \end{aligned} \quad (5)$$

When the integration is performed, the ratio of the r dependent canonical functions is monitored until saturation with respect to r is reached at both limits ($r \rightarrow 0$ and $r \rightarrow \infty$). The saturation of the $\frac{\alpha(E; r)}{\beta(E; r)}$ ratio with r yields a position independent eigenvalue function $F(E)$. The latter is mathematically defined with the help of two associated energy functions:

$$l_-(E) = \lim_{r \rightarrow 0} -\frac{\alpha(E; r)}{\beta(E; r)} \quad (6)$$

and:

$$l_+(E) = \lim_{r \rightarrow +\infty} -\frac{\alpha(E; r)}{\beta(E; r)} \quad (7)$$

as:

$$F(E) = l_+(E) - l_-(E) = \left[\frac{y'(r_0)}{y(r_0)} \right]_+ - \left[\frac{y'(r_0)}{y(r_0)} \right]_- \quad (8)$$

its zeroes expressing the continuity of $y(r)$ and its derivative $y'(r)$ at the point r_0 (matching conditions) yield the spectrum of the RSE. In practice we have:

$$l_-(E) \approx -\frac{\alpha(E; r_{min})}{\beta(E; r_{min})} \quad (9)$$

and:

$$l_+(E) \approx -\frac{\alpha(E; r_{max})}{\beta(E; r_{max})} \quad (10)$$

with r_{min}, r_{max} the radial coordinates where saturation is observed (within some predefined tolerance) respectively in $l_-(E)$ and $l_+(E)$. An example of typical behaviour of $F(E)$ is displayed in Fig. 1. The eigenfunctions may be obtained for any $E = E_k$ where E_k is a zero of $F(E)$.

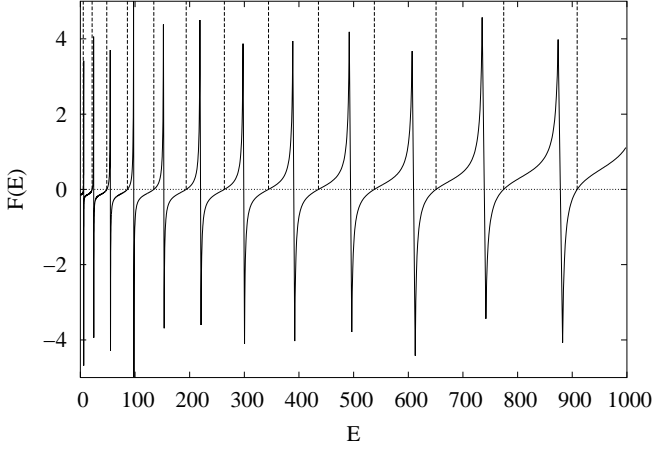


FIG. 1 Typical behavior of the eigenvalue function with energy. The vertical lines indicate the eigenvalue position. The graph of the eigenvalue function has an approximate $\tan(E)$ shape versus the energy E .

The eigenvalue function definition depends on the type of boundary conditions at hand. In the Appendix we describe the general boundary conditions case and the corresponding matching conditions along with the corresponding eigenvalue function.

The $\tan(E)$ shape of $F(E)$ provides a deep insight into the physical significance of the CFM method. The latter transforms a SBVP from the open interval $[0, \infty[$ to the finite interval $[r_{min}, r_{max}]$ defined by the saturation coordinates of the energy functions. This means the CFM maps an arbitrary potential $V(r)$ onto the infinite square well problem defined by $V(r) = 0$ in the open interval $]r_{min}, r_{max}[$ and $V(r_{min}) = V(r_{max}) = \infty$ (see section VII for additional information). In fact, for the infinite square well problem $F(E)$ has a $\tan(E)$ (see also ref. (25)).

The speed and accuracy of the CFM method have been tested and compared to standard integration algorithms such as the order four Runge-Kutta (RK4) method, Numerov etc.. in a variety of cases and for a wide of range of potentials.

More specifically, r_0 being selected as the starting point for the integration, the r -axis is divided into intervals $I_p = [r_p, r_{p+1}]$ in a way such that the potential can be series expanded over I_p (see refs (16; 17)).

The expansion uses coefficients $\gamma_n^{(p)}$ so that the local ex-

pression of the total potential is defined as:

$$\left[V(r) + \frac{l(l+1)}{r^2} \right]_{r \in I_p} = \sum_{n=0}^{\infty} \gamma_n^{(p)} x^n, x \in I_p \quad (11)$$

In order to perform integration, we use the following variable step difference equation:

$$y_{p+1} = y_p + h_p y'_p + \sum_{n=2}^{\infty} C_n^{(p)} h_p^n \quad (12)$$

$$y'_{p+1} = y'_p + \sum_{n=2}^{\infty} n C_n^{(p)} h_p^{n-1} \quad (13)$$

where the $y_p = y(r)$ are a particular set of canonical functions and the $y'_p = y'(r)$ are their derivatives in the interval $[r_p, r_{p+1}]$. The $C_n^{(p)}$ are given by the recursion formula for energy E obtained from series expanding eq. 3:

$$(n+2)(n+1)C_{n+2}^{(p)} = \sum_{m=0}^n C_m^{(p)} \gamma_{n-m}^{(p)} - E C_n^{(p)} \quad (14)$$

with $C_0^{(p)} = y_p$ and $C_1^{(p)} = y'_p$.

In practice, the above sums over n are truncated to a cutoff value N (instead of ∞) chosen large enough so that the remainder error is less than a selected truncation error ϵ_T .

Given N and ϵ_T , the integration step h_p for the interval $[r_p, r_{p+1}]$ is deduced from $h_p = (\epsilon_T^2 / |C_N^{(p)}|)^{\frac{1}{N}}$.

At the starting point of integration r_0 , the starting step size h_0 is thus determined, and the procedure is repeated at $r_1 = r_0 + h_0$ leading to h_1 and so forth until we reach $r_{p+1} = r_p + h_p$ after p steps.

These equations allow the propagation of the solution from one point to the next using a variable step and a local series expansion of variable order controlled by the truncation error ϵ_T . The accuracy of the results are monitored with respect to the decrease of ϵ_S and the procedure is referred to as the VSCA (Variable Step with Controlled Accuracy) method.

Generally, one avoids using or evaluating the radial wavefunction but if one insists on evaluating it, the canonical functions $\alpha(E; r)$ and $\beta(E; r)$ are used to determine the radial wavefunction at any energy via the expression:

$$u_l(E; r) = u_l(E; r_0) \alpha(E; r) + u'_l(E; r_0) \beta(E; r) \quad (15)$$

where $u_l(E; r)$ and $u'_l(E; r_0)$ are the radial wavefunction and its derivative at the initial distance r_0 .

Before proceeding any further, the essential test of any method that pretends solving the RSE is the Coulomb

potential and the essential case to test the accuracy and reliability of the CFM is the (textbook) Hydrogen atom.

The CFM results are shown in Table. I along with the exact analytical results.

Index	CFM (Ry)	Exact (Ry)
1	-1.00000	-1.00000
2	-0.250000	-0.250000
3	-0.111111	-0.111111
4	-6.25000(-2)	-6.25000(-2)
5	-4.00000(-2)	-4.00000(-2)
6	-2.77778(-2)	-2.77778(-2)
7	-2.04082(-2)	-2.04082(-2)
8	-1.56250(-2)	-1.56250(-2)
9	-1.23457(-2)	-1.23457(-2)
10	-1.00000(-2)	-1.00000(-2)
11	-8.26446(-3)	-8.26446(-3)
12	-6.94444(-3)	-6.94444(-3)
13	-5.91716(-3)	-5.91716(-3)
14	-5.10204(-3)	-5.10204(-3)
15	-4.44445(-3)	-4.44445(-3)
16	-3.90625(-3)	-3.90625(-3)
17	-3.46021(-3)	-3.46021(-3)
18	-3.08642(-3)	-3.08642(-3)
19	-2.77008(-3)	-2.77008(-3)
20	-2.50000(-3)	-2.50000(-3)
21	-2.26757(-3)	-2.26757(-3)
22	-2.06612(-3)	-2.06612(-3)
23	-1.89036(-3)	-1.89036(-3)
24	-1.73611(-3)	-1.73611(-3)

TABLE I Energy levels of the Hydrogen atom. Middle column values are the CFM results whereas the last column values are the corresponding exact analytically obtained values. The numbers in parenthesis represent a power of 10.

It is remarkable to notice that all digits (calculated by CFM and analytically) are all same.

The classical Morse potential is the simplest model for the evaluation of vibrational spectra of diatomic molecules. First of all, we have analytical expressions for the levels, secondly it provides a stringent test of the CFM before embarking into more sophisticated cases such as weakly bound or cold molecules (also called long-range molecules).

The Morse potential is given by:

$$V(r) = D[1 - \exp(-a\{r - r_e\})]^2 - D \quad (16)$$

with the values D, a, r_e equal respectively to 188.4355, 0.711248, 1.9975 in au. The analytic expression for the levels is:

$$E_n = -\frac{a^2 \hbar^2}{2\mu} (\sqrt{2\mu D}/a - n - 1/2)^2, \quad (17)$$

with $\max n \leq \sqrt{2\mu D}/a - 1/2$. Hence the number of levels is given by: $N = \sqrt{2\mu D}/a - 1/2$.

Working with units such that $\hbar = 1$ and $2\mu = 1$, the Morse potential and the eigenvalue function $F(E)$ are displayed in the figures below. The table contains the levels calculated by CFM and compared to the analytical case. Again, like in the pure Coulomb case treated previously, the agreement is perfect and we found all the levels ($N = 19$) as predicted analytically.

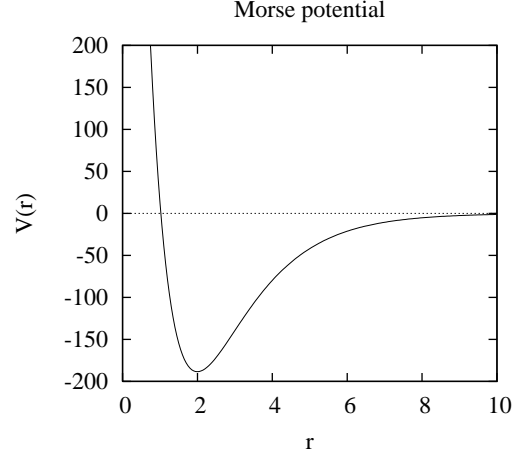


FIG. 2 Morse potential $V(r) = D[1 - \exp(-a\{r - r_e\})]^2 - D$ with parameters $D = 188.4355$, $a = 0.711248$, $r_e = 1.9975$.

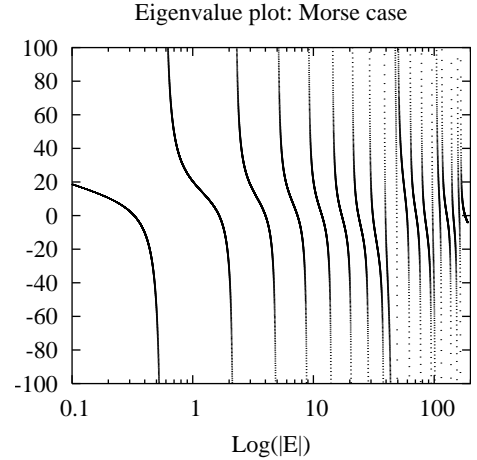


FIG. 3 Behavior of the eigenvalue function $F(E)$ with energy on a semi-log scale for the Morse potential.

A. The Multichannel case

The CFM can be extended to the multichannel (or multi-component) problem, where the functions $\alpha(E; r)$

Index	CFM	Exact
1	-178.798248	-178.798538
2	-160.282181	-160.283432
3	-142.778412	-142.78006
4	-126.287987	-126.288445
5	-110.807388	-110.808578
6	-96.3395233	-96.3404541
7	-82.8832169	-82.884079
8	-70.4389801	-70.4394531
9	-59.0056	-59.0065727
10	-48.5851288	-48.5854378
11	-39.1754532	-39.1760521
12	-30.77771	-30.7784157
13	-23.3919983	-23.3925247
14	-17.0183048	-17.018383
15	-11.6557436	-11.6559868
16	-7.3050122	-7.30533791
17	-3.9661877	-3.9664371
18	-1.6390723	-1.63928342
19	-0.3238727	-0.32387724

TABLE II Energy levels of the Morse potential $V(r) = D[1 - \exp(-a\{r - r_e\})]^2 - D$ with parameters $D = 188.4355$, $a = 0.711248$, $r_e = 1.9975$. Middle column values are the CFM results whereas the last column values are the corresponding exact analytically obtained values. Units are such that $\hbar = 1$ and $2\mu = 1$.

and $\beta(E; r)$ are no longer scalar functions of E and r . Multichannel case occurs when we have a potential well with several local minima or when we are dealing with Scattering problems requiring simultaneously incident and scattered wavefunctions. In addition, spin leads naturally to multicomponent wavefunctions.

Starting from a Schrödinger system of equations of the form:

$$\sum_{k=1}^N F_{ik} y_k(r) = 0, \quad i = 1, 2, \dots, N \quad (18)$$

where:

$$\begin{aligned} F_{ik}(r) &= (2\mu/\hbar^2) V_{ik}(r) \\ F_{ii}(r) &= (2\mu/\hbar^2) (-d^2/dr^2 - E_i + V_{ii}(r)) \end{aligned} \quad (19)$$

The elements $F_{ik}(r)$ of the matrix F are physical operators and the unknown functions $y_k(r)$ are partial radial waves satisfying the boundary conditions at $r = 0$ and $r = \infty$:

$$y_k(r = 0) = y_k(r = \infty) = 0 \quad \forall k \quad (20)$$

Following Friedman and Jamieson (18), we rewrite the N -component equation as a set of N coupled Schrödinger equations for a matrix potential with elements $V_{ij}(r)$:

$$y_i''(r) + (2\mu/\hbar^2)[E - V_{ii}(r)]y_i(r) = (2\mu/\hbar^2) \sum_{k=1}^N V_{ik} y_k(r) \quad (21)$$

where $i, k = 1, 2, \dots, N$.

Using linear superposition, we can write the full solution as:

$$y(r) = \sum_{k=1}^N [y_k(r_0) \alpha_{ik}(E; r) + y_k'(r_0) \beta_{ik}(E; r)] \quad (22)$$

where, as before, r_0 is an arbitrary point between zero and infinity, $\alpha_{ik}(E; r)$, $\beta_{ik}(E; r)$ are $2N$ independent particular solutions satisfying the set of initial conditions:

$$\begin{aligned} \alpha_{ik}(E; r_0) &= \beta_{ik}'(E; r_0) = \delta_{ik} \\ \alpha_{ik}'(E; r_0) &= \beta_{ik}(E; r_0) = 0 \end{aligned} \quad (23)$$

Going from the indicial to the matrix representation, we can build a matrix $\mathbf{L}(\mathbf{E}, \mathbf{r})$ that depends on the energy E and radial position r defined by:

$$\mathbf{L}(\mathbf{E}, \mathbf{r}) = \beta^{-1}(\mathbf{E}, \mathbf{r}) \alpha(\mathbf{E}, \mathbf{r}) \quad (24)$$

where α and β are $N \times N$ matrices whose elements are the $\alpha_{ik}(E; r)$, $\beta_{ik}(E; r)$ functions.

The analogue of the eigenvalue function is now given by the determinant equation:

$$D(E) = |\mathbf{L}(\mathbf{E}, \mathbf{0}) - \mathbf{L}(\mathbf{E}, \infty)| \quad (25)$$

The eigenvalues are given by the zeroes of the determinant $D(E) = 0$.

Let us apply the above to the particular case where the matrix potential $V(r)$ (18) is a constant coupling matrix \mathbf{C} multiplying a scalar function $M(r)$:

$$\mathbf{V}(r) = \mathbf{C}M(r), \quad V_{ij} = C_{ij}M(r), \quad i, j = 1, \dots, 6 \quad (26)$$

The r dependence is contained solely in the radial function $M(r) = z^2 - 2z$, $z = \exp(-ax)$, $x = r - r_e$ where r_e is the scalar potential (minimum) equilibrium value. \mathbf{C} is a full (6×6) constant matrix that may be diagonalised by the similarity transformation: $\mathbf{C} = \mathbf{Q} \mathbf{G} \mathbf{Q}^{-1}$. \mathbf{Q} is a non-singular real constant matrix and \mathbf{G} is a (6×6) diagonal matrix. Picking a coupling matrix \mathbf{C} similar to a diagonal matrix \mathbf{G} whose elements G_{ii} , $i = 1..6$ are respectively: $\{24, 31.5, 37.5, 42, 56, 63\}$, the initial fully coupled six-channel problem 26 is transformed into six uncoupled Schrödinger equations that are solved with

the multichannel CFM. The full spectrum of $V(r)$ is made from the union of the sets of eigenvalues of the six individual Schrödinger equations.

In order to benchmark the CFM results, we note that this multichannel example is nothing other than a special matrix form of the Morse potential. Then, we have access to the full spectrum analytically as in the scalar Morse case:

$$E_{in} = -w_e x_e (d_i - n - 1/2)^2, \quad i = 1, \dots, 6, n \leq d_i - 1/2, \quad (27)$$

where $d_i = \sqrt{(G_{ii}/w_e x_e)}$ and $w_e x_e = a^2 \hbar^2 / 2\mu$. In order to perform a detailed numerical comparison between the numerical performance of the CFM and the multichannel Morse potential analytical results, we take: $r_e = 1.5 \text{ \AA}$, $w_e x_e = 8 \text{ cm}^{-1}$ and $a = 1.540 \text{ \AA}$. The comparison between the computed and the exact eigenvalues displayed in table III shows that they are almost indistinguishable.

(i, n)	Exact	CFM
(6,0)	-42.550 055 679 356	-42.550 055 679 344
(5,0)	-36.833 989 511 483	-36.833 989 511 484
(4,0)	-25.669 697 220 176	-25.669 697 220 173
(3,0)	-22.179 491 924 311	-22.179 491 924 313
(2,0)	-17.625 492 133 612	-17.625 492 133 614
(6,1)	-13.650 167 038 069	-13.650 167 038 068
(1,0)	-12.143 593 539 448	-12.143 593 539 445
(5,1)	-10.501 968 534 449	-10.501 968 534 446
(4,1)	-5.009 091 660 529	-5.009 091 660 528
(3,1)	-3.538 475 772 933	-3.538 475 772 933
(2,1)	-1.876 476 400 837	-1.876 476 400 834
(6,2)	-.750 278 396 781	-.750 278 396 781
(1,1)	-.430 780 618 346	-.430 780 618 346
(5,2)	-.169 947 557 416	-.169 947 557 416

TABLE III Analytical and Multi-channel CFM computed eigenvalues E_{in} . All values are in cm^{-1} .

B. Evaluation of energy spectra and phaseshift

Before treating any problem with the CFM a number of constraints should be underlined in order to properly tackle any problem with this method whether it pertains to energy spectra evaluation or phaseshift:

- General considerations:
 - The potential is spherically symmetric.
 - The interval of interest should be of infinite length.

- Ill-conditioning and accuracy: The spectrum depends on the zeroes of $F(E) = l_+(E) - l_-(E)$. This subtraction leads to inaccuracies because the entire spectrum depends on the zeroes of $F(E)$ in the single channel case or $D(E) = |\mathbf{L}(\mathbf{E}, \mathbf{0}) - \mathbf{L}(\mathbf{E}, \infty)|$ in the multichannel case.
- r_0 issue and the number of eigenvalues: The number of eigenvalues depend strongly on r_0 . r_0 should be increased until a $\tan(x)$ like diagram for the energy function is obtained. For short-range potentials, r_0 should be close to the minimum of the potential or the equilibrium value of the radial distance r_e . If r_0 is far from minimum, it will see only those levels close to the value of $V(r_e)$.

- Energy spectra calculations:

- The method being sensitive to convergence for $r \rightarrow 0$ and $r \rightarrow \infty$, One has to check that for $r \rightarrow 0$ the canonic functions α and β are diverging near the origin in the same way (saturation of the ratio).
- One has to check that for $r \rightarrow \infty$ the canonic functions α and β have reached their Asymptotic behaviour (of the Coulombic form $\sin(kr)/kr$).
- Note:** This is not true for the phase.
- One should have a regular structure of the $\tan(E)$ type for the energy function $F(E) = l_+(E) - l_-(E)$ in the single channel (or $D(E) = |\mathbf{L}(\mathbf{E}, \mathbf{0}) - \mathbf{L}(\mathbf{E}, \infty)|$ in the multichannel case).
- The method is very sensitive to r_0 .
- Forward integration step $r \rightarrow \infty$: typically it is 0.1 to 1 in energy calculations. In phase calculations it is 0.1 to 0.01. It is sensitive to the energy used. When the energy increases the step should be decreased. There is a compromise to be reached because if the step is too much reduced any physical quantity will saturate immediately.

- Phaseshift calculations:

- The phase stability might be reached long before the asymptotic regime in $\Psi(E; r) \sim \sin(kr)/kr$ is reached. Typically the phase is stable when the potential is about 0.1 au.
- One has to check that for $r \rightarrow 0$ the canonic functions α and β are diverging near the origin in the same way (saturation of the ratio).
- The method being very sensitive to r_0 , we ought to treat separately the different types of potential. The general rules are enunciated below:

- * Short-range potentials: Typically $r_0 \sim 1$ for all angular momentum L and energies. For large energies r_0 should be reduced.
- * Long-range potentials: Typically $r_0 \sim 1$ for all L but for small energies (1-10 au). For large energies r_0 should be reduced to 0.1.
- Bessel functions are used for Short-range potentials only. Trigonometric functions are used for Long-range and Short-range potentials potentials.
- Forward integration step $r \rightarrow \infty$: typically it is 0.1 to 1 in energy calculations. In phase calculations it is 0.1 to 0.01. It is sensitive to the energy used. When the energy increases the step should be decreased. There is a compromise to be reached because if the step is too much reduced any physical quantity will saturate immediately.
- The stability of the CFM is based on the following: two independent sets of solutions are generated at some central point, integrating inwards to the origin and outwards to the asymptotic region. Both contain linear combinations of the regular and the irregular solutions, and by suitably combining them, the irregular solution is eliminated. Integration can be made out to a very large radius, allowing the phaseshift to be determined by matching to plane or Coulomb wave solutions. It is not necessary to obtain a series expansion of the solution in order to start the integration, making it unnecessary to series expand the potential.
- The method can be successfully applied to scattering problems where the phaseshift is of paramount importance in the determination of the scattering cross section. Of particular importance are (e,2e) scattering problems that are dealt with in section VII.

A final point to consider when dealing with the CFM using standard integration methods is that one cannot in general proceed toward the origin $r = 0$ because of the potential singularity (for instance, the RK method blows up at $r = 0$) in contrast with the VSCA algorithm.

III. POTENTIAL ESTIMATION FROM SPECTROSCOPY

The high accuracy of the CFM allows to retrieve the potential (in parametric or pseudo form) from the observed atomic or molecular spectra. We exploit the Quantum Defect (QD) as an indicator of the results obtained by the CFM in order to find the optimal parameters of the potential.

QD information is widely exploited in modern spectroscopy, to characterize Rydberg states and in the calculation of the photoionization cross sections of various atomic and molecular species (1; 27).

We show in this section that QD information, used within the Distorted Wave Born Approximation (DWBA) framework (62), might also prove useful for the description of ionization processes by presenting an alternative way to account for the short range interactions (static and exchange) in the calculation of the final state continuum distorted waves. The range of validity of this approach reaches beyond that (51) of the commonly used Furness-McCarthy local exchange approximation (19). Compared to the determination of the Hartree-Fock non-local operator (63), which becomes rapidly a tedious task as the size of the target increases, our method allows for a target-independent procedure which can be readily applied to much larger atomic or molecular systems.

The parameters of the Green-Sellin-Zachor (21) parametric form of the electron-ion potential are optimized in order to reproduce the QD using the CFM (29). Several parametric potentials are discussed extensively in the literature and we already used several functional forms (1) adapted to different atomic systems. We have studied (59) the QD of some rare gases with the Klapisch parametric potential (28) and found that in some cases it was very difficult to optimize parameters that provide an accurate representation of the experimental QD. We believe, the Green-Sellin-Zachor (21) is better suited to our present study as the parameter space is small (two-dimensional) which allows for an efficient search of the optimized parameters.

The electron-ion potentials obtained for each Rydberg series are further modified to account classically for the electron-electron interaction in the final state. Calculations performed within the DWBA framework for the ionization of argon in the equal energy sharing geometry $\mathbf{k}_a = -\mathbf{k}_b$, which is reasonably well documented both theoretically and experimentally, clearly validate our approach and shows significant improvements over previous treatments.

A. Optimisation procedure

An extensive review of the applications of model potentials has been given by Hibbert (24) and Aymar *et al.* (1). The functional form suggested by Green *et al.* (21) is given by:

$$V(r) = -(2/r)[(Z-1)\omega(r) + 1],$$

$$\text{with } \omega(r) = 1/[\epsilon_1(\exp(r/\epsilon_2) - 1) + 1] \quad (28)$$

where ϵ_1 and ϵ_2 are parameters that are determined by the optimisation procedure.

The optimisation problem, at hand, is over-determined since the experimental set of energy levels might consist of tens of values whereas the potential depends only on two numbers, namely ϵ_1 and ϵ_2 . This over-determination allows us to use several criteria for the optimisation procedure and later on select the best one that achieves results closest to experiment.

The optimization procedure consists of defining an objective function and finding its minimum in the two-dimensional parameter space ϵ_1, ϵ_2 . The objective function is a quadratic consisting of the difference between some picked levels and those produced by the parametric potential through the solution of the RSE with the CFM.

We adopted several strategies based on the following observations: The QD value is not stable for the low levels but tends to reach a stable value when the energy increases. Despite the stability of the QD for the higher levels, the experimental (and therefore) numerical accuracy decreases when the energy increases.

Therefore a compromise should be achieved by selecting the levels in order to define the objective function to minimize.

We found that a reasonable compromise should be based on the following operations that differ with the selected rare gas:

1. Pick some level and take the average of a number of higher ones.
2. Pick two high levels for which the QD has stabilised within a given accuracy.
3. Pick a low level and a high one for which the QD has already stabilised.

All the above operations should yield roughly the same values for the parameters before running the final check in order to test the accuracy of the obtained eigenvalues.

Series	ϵ_1	ϵ_2
$l=0$	3.625	1.036
$l=1$	3.62	1.06
$l=2$	3.6344	1.036

TABLE IV Szydluk-Green parameters for the first three Rydberg series of Argon.

The optimization program itself is based on a globally convergent method for solving non-linear system of equations: the multidimensional secant method developed by Broyden (9). It is based on a fast and accurate

method for the iterative evaluation of the Jacobian of the objective function needed during the minimisation procedure.

It is a Quasi-Newton method that consists of approximating the Jacobian and updating it with an iterative procedure. It converges superlinearly to the solution like all secant methods.

There are several ways to perform the integration of the RSE on the basis of the CFM. One may use a fixed step scheme such as the explicit RK4 method or a variable step (VSCA) procedure. Optimization wise, the RK4 method is faster than VSCA but less accurate. To judge the accuracy of our optimization we compare in table IV our results for the energy levels and corresponding QD obtained using the RK4 and VSCA integration scheme with those of Szydluk *et al.* (58). The results displayed in table IV clearly favor, as expected, the VSCA integration scheme. In contrast to the VSCA, the RK4 integration scheme is limited to fourth order accuracy. Table IV further shows the sensitivity of the QD to the numerical values of the calculated energy levels. Despite small differences between the energy values obtained with the RK4 and VSCA methods, the corresponding QD's largely differ. This sensitivity of the QD is the main motivation for using it rather than the raw energy levels in our optimization procedure.

Experimental levels	RK4	VSCA
-0.309522	-0.214082	-0.310563
-0.124309	-9.87422(-2)	-0.124506
-6.76780(-2)	-5.69743(-2)	-6.76904(-2)
-4.25540(-2)	-3.70845(-2)	-4.25546(-2)
-2.92210(-2)	-2.60593(-2)	-2.92238(-2)
-2.13080(-2)	-1.93126(-2)	-2.13062(-2)
-1.62200(-2)	-1.48846(-2)	-1.62210(-2)
-1.27620(-2)	-1.18223(-2)	-1.27614(-2)
-1.03020(-2)	-9.61654(-3)	-1.03015(-2)
-8.49000(-3)	-7.97521(-3)	-8.49011(-3)
-7.11800(-3)	-6.72092(-3)	-7.11771(-3)

TABLE V Comparison between the experimental and calculated energy levels of the Rydberg series of Argon. The levels calculated with the CFM are obtained either with fixed step (RK4) or variable step (VSCA) integration. All values in Rydbergs.

IV. VIBRATIONAL SPECTRA OF COLD MOLECULES

A new kind of high precision molecular spectroscopy is probing long-range forces between constituent atoms of molecules. This spectroscopy is based on using light to combine two colliding cold-trapped atoms into a tenuous molecule.

Experimental QD	RK4	VSCA
0.202561	0.838726	0.205576
0.163723	0.817645	0.165967
0.156063	0.810516	0.156415
0.152366	0.807174	0.152400
0.150046	0.805324	0.150326
0.149399	0.804191	0.149110
0.148104	0.803444	0.148345
0.148016	0.802940	0.147808
0.147664	0.802574	0.147425
0.147091	0.802298	0.147161
0.147199	0.802084	0.146957

TABLE VI Comparison between the experimental and calculated QD of the Rydberg series of Argon. The levels calculated with the CFM are obtained either with fixed step (RK4) or variable step (VSCA) integration.

The burgeoning field of "Photoassociation Spectroscopy" is allowing very precise measurement of lifetimes of the first excited states of Alkaline atoms and observation of retardation effects and long-range forces. It provides a means of probing accurately the weak interaction between these atoms (26).

The agreement between theory and experiment requires simultaneously a highly accurate representation of the interaction potential as well as a highly reliable method for the calculation of the corresponding energy levels.

Since our aim is directed towards the latter problem, we make use of an alternative method to evaluate the energy levels for the potential at hand instead of comparing to the experimental values in order to assess the validity of our results.

The determination of the vibrational spectra of these very tenuous molecules is extremely subtle specially for the highest levels which play an important role in photoassociation spectroscopy. Thus a careful control of accuracy is needed in order to diagonalise the Hamiltonian without losing accuracy for all energies including those close to the dissociation limit.

The magnitudes of potential energy, distance and mass values in these kinds of molecules stand several orders of magnitude above or below what is encountered in ordinary short-range molecules.

For instance, the typical intramolecular potential well depth at the equilibrium distance of about 100 a_0 (Bohrs), is a fraction of a cm^{-1} while the reduced mass is several 10,000 electron masses. All these extreme values require special numerical techniques in order to avoid roundoffs, divergences, numerical instability and ill-conditioning during processing.

As a first example, Johnson et al. (25) introduced a variant of the Morse potential with parameters given by $D = 0.142, a = 0.815, r_e = 2.835$. While the mass pa-

rameter in the Morse case is $0.5 m_e$, in the Johnson case it is very large and equal to $9114.44 m_e$.

Large values of the mass parameter lead to a very shallow well in the potential energy (see fig. 4) that means a very small binding energy making the molecule extremely weak. This then corresponds to the so-called long-range or cold molecule because of the extremely low molecular binding energy. In addition the potential width around the minimum is very broad implying large quantum fluctuations in the ground state in contrast to the ordinarily deep and narrow Morse potential.

The potential energy is given by:

$$V(r) = D[1 - \exp(-a\{r - r_e\})]^2 - D \quad (29)$$

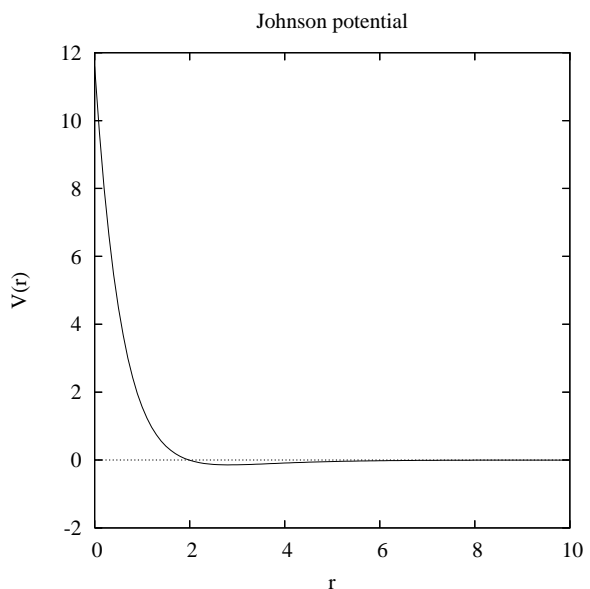


FIG. 4 Johnson potential versus distance. The Morse parameters are $D = 0.142, a = 0.815, r_e = 2.835$. Note the shallowness and breadth of the potential minimum. We use the same units as the Morse potential described previously in fig. 2.

In order to perform the eigenvalue calculation we rescale the parameters $D = 0.142, a = 0.815, r_e = 2.835$ such that they are as close as possible to the Morse potential described previously. The scaling yields the parameters: $D = 142.387, a = 0.815131, r_e = 2.83459$. These values yield in a straightforward way all the eigenvalues (62 in total), the first thirty only being displayed in Table VII.

A. Vibrational energy levels of the $^{23}\text{Na}_2$ molecule

Since vibrational spectra of the Johnson molecule is determined accurately and to arbitrary accuracy with the CFM, we move on to tackle the $^{23}\text{Na}_2$ molecule. The

Index	Exact	CFM	Johnson
0	497.668182	497.726562	498.
1	1481.66138	1481.67773	1482.
2	2449.65503	2449.69922	2450.
3	3401.64697	3401.70508	3402.
4	4337.6416	4337.69531	4338.
5	5257.63672	5257.68164	5258.
6	6161.63232	6161.66016	6162.
7	7049.62842	7049.63672	7050.
8	7921.62256	7921.67969	7922.
9	8777.62012	8777.70508	8778.
10	9617.61719	9617.67578	9618.
11	10441.6133	10441.6348	10442.
12	11249.6113	11249.6504	11250.
13	12041.6084	12041.6914	12042.
14	12817.6074	12817.6465	12818.
15	13577.6055	13577.6445	13578.
16	14321.6045	14321.666	
17	15049.6045	15049.6191	
18	15761.6035	15761.666	
19	16457.6035	16457.6484	
20	17137.6055	17137.6523	
21	17801.6055	17801.6484	
22	18449.6074	18449.6328	
23	19081.6094	19081.6562	
24	19697.6113	19697.6406	
25	20297.6152	20297.666	
26	20881.6172	20881.6562	
27	21449.6211	21449.6602	
28	22001.625	22001.668	
29	22537.6289	22537.6328	

TABLE VII First thirty vibrational levels of the Johnson diatomic molecule in cm^{-1} . Johnson results (limited to the first sixteen only) are compared to the CFM and the exact values. The corresponding analytical values are almost indistinguishable (see ref. (25)). The total number of levels is 62 with the parameters $D = 0.142$, $a = 0.815$, $r_e = 2.835$.

energy levels of the 0_g^- and 1_u electronic states of the $^{23}\text{Na}_2$ molecule are determined from the Ground state up to the continuum limit. The method is validated by comparison with previous results obtained by Stwalley *et al.* (57) using the same potential and Trost *et al.* (60) whose work is based on the Lennard-Jones potential adapted to long-range molecules.

The method we use in this work adapts well to this extreme situation with the proviso of employing a series of isospectral scaling transformations we explain below.

We apply the CFM to the calculation of the vibrational energy levels of a diatomic molecule where the interaction between the atoms is given by the Movre and Pichler potential (42).

We start with the 0_g^- electronic state of the $^{23}\text{Na}_2$ molecule. The corresponding potential is given by:

$$V(r) = \frac{1}{2}[(1 - 3X) + \sqrt{1 - 6X + 81X^2}] \quad (30)$$

where $X = \frac{C(0_g^-)}{9r^3\Delta}$. r is the internuclear distance and the parameter $C(0_g^-)$ is such that:

$$\lim_{r \rightarrow +\infty} V(r) \rightarrow -\frac{C_3(0_g^-)}{r^3} \quad (31)$$

Identification of the large r limit yields the result: $C_3(0_g^-) = C(0_g^-)/3$. In the calculations below, we have used $C_3(0_g^-) = 6.390$ Hartrees. a_0^3 like Stwalley *et al.* (57). The parameter $\Delta = 1.56512 \cdot 10^{-4}$ Rydbergs is the atomic spin-orbit splitting. Given $C_3(0_g^-)$ and Δ , the equilibrium internuclear distance is $r_e = 71.6a_0$.

The peculiarities of the 0_g^- and 1_u electronic states of the $^{23}\text{Na}_2$ molecule are evident in fig. 5. The 1_u state is higher than the 0_g^- and the number of vibrational levels is smaller because the potential is shallower. This has important consequences as we explore the vibrational spectrum below.

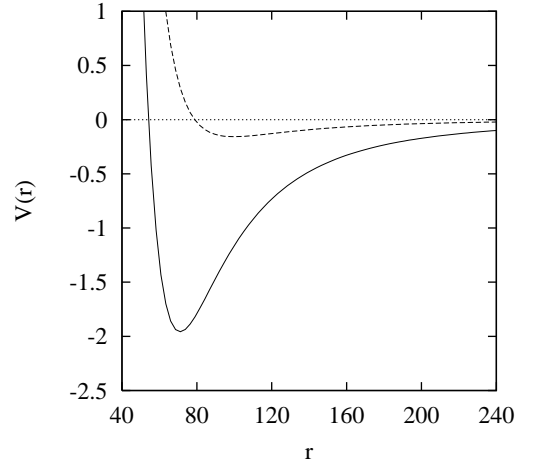


FIG. 5 Potential energy in cm^{-1} for the 0_g^- and 1_u electronic states (upper shallow curve) of the $^{23}\text{Na}_2$ molecule. The radial distance r is in Bohrs (a_0) units.

We scale all energies with a factor E_0 (usually cm^{-1}) with the use of equation (1). Then we scale all distances with a typical length L_0 transforming the RSE appropriately. This double transformation is reflected generally in the potential coefficients preserving thus the functional form of the potential.

In order to gauge the accuracy of the spectra, we perform the integration of the RSE with two different methods: the fixed step RK4 and the variable step VSCA methods (35).

The VSCA method is based on a series expansion of the potential and the corresponding solution to an order

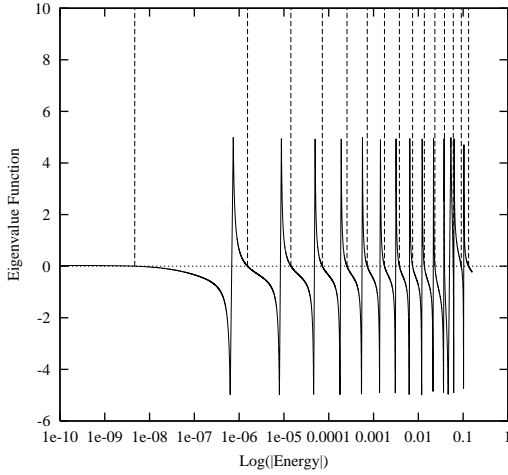


FIG. 6 Behavior of the eigenvalue function $F(E)$ with energy on a semi-log scale for the 1_u electronic state of the $^{23}\text{Na}_2$ molecule. The vertical lines indicate the eigenvalue position. Energies are in cm^{-1} .

such that a required tolerance criterion is met. Ideally, the series coefficients are determined analytically to any order, otherwise loss of accuracy occurs leading quickly to numerical uncertainties as discussed later.

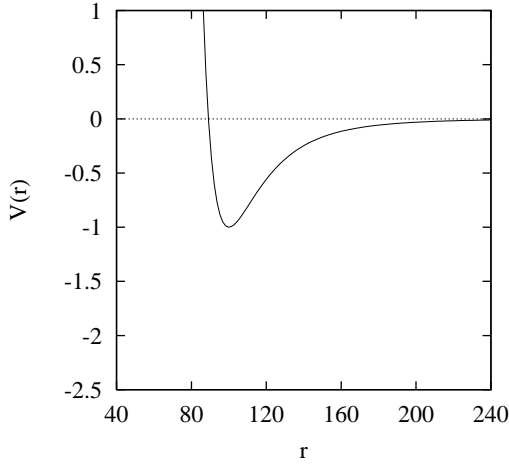


FIG. 7 Potential energy of the Trost *et al.* (60) model. The energy is in ϵ units where ϵ is the potential well depth and the radial distance is in $\frac{a_0}{\sqrt{B}}$ where B is a scaled mass. We use the same interval for the potential and radial distance in order to ease the comparison with fig. 5 pertaining to the $^{23}\text{Na}_2$ molecule.

Table VIII shows the results we obtain with the RK4 method. The limitation of the RK4 method to fourth order hampers the finding of levels beyond the 33rd (see table VIII). In order to find the higher levels we have to select an algorithm that enables us to tune the accuracy well beyond the fourth order.

Pushing the accuracy within the framework of a fixed step method has the effect of reducing substantially the

integration step. In order to avoid this problem, we use a variable step that adjusts itself to the desired accuracy, the VSCA method.

This method is powerful and flexible enough to find all the desired energy levels and allows us to find one additional level that was not detected before. It should be noted that the last three levels given by Stwalley *et al.* (57) were extrapolated and not calculated. The agreement between our calculated levels and those of Stwalley *et al.* (57) is quite good. We believe that the small discrepancy, increasing as we progress towards the dissociation limit, is due to a loss of accuracy associated with traditional methods in sharp contrast with the CFM.

The estimation of accuracy of the results hinges basically on two operations, integration and determination of the zeroes of the eigenvalue function $F(E)$. The superiority of the VSCA method is observed in the determination of the upper levels that are not detected by the RK4 method (see Tables 1 and 2). In addition, it is observed in the behavior of the eigenvalue ratio versus the index. While in both cases (RK4 and VSCA) the ratio increases steadily as the index increases because we are probing higher excited states, in the RK4 case it rather blows up as dissociation is approached. We use typically series expansion to order 12 in VSCA with a tolerance of 10^{-8} . In the root search of $F(E)$, the tolerance required for a zero to be considered as an eigenvalue is 10^{-15} . This does not imply that we disagree as strongly as 0.13%, for instance, with the Ground state value (see Tables 1 and 2) found by Stwalley *et al.* (57) for the simple reason, we use a splitting energy $\Delta = 1.56512 \cdot 10^{-4}$ Rydbergs corresponding to an equilibrium internuclear distance $r_e = 71.6a_0$. Stwalley *et al.* do not provide explicitly the value of Δ they use, however Jones *et al.* (26) use a value that is slightly different.

We move on to treat the 1_u electronic state of the $^{23}\text{Na}_2$ molecule. The potential associated with the 1_u electronic state of the $^{23}\text{Na}_2$ molecule is a lot more involved. Its VSCA implementation is particularly difficult because of the complex functional of the potential as we explain below. Analytically, the VSCA algorithm requires performing a Taylor series expansion to any order around an arbitrary point (31).

Numerically, this is still an open problem for arbitrary functions. If one turns toward the use of LISP based symbolic manipulation techniques cumbersome expressions are produced hampering any progress. Special methods based on analytical fitting expressions are needed in order to turn the series coefficients into a more manageable form (see refs (16; 17)).

The first step is to determine the 1_u electronic state of the $^{23}\text{Na}_2$ molecule by solving the Movre *et al.* (42) secular equation such that:

$$V(r) = \Delta \left[-2\sqrt{Q} \cos\left(\frac{\theta - 2\pi}{3}\right) - \frac{a}{3} - 1 \right] \quad (32)$$

where $a = -2 - 6X$ and $X = \frac{C(1_u)}{9r^3\Delta}$. In addition, $\theta =$

Index	RK4 (cm ⁻¹)	Stwalley <i>et al.</i> (cm ⁻¹)	Ratio
1	-1.7864563	-1.7887	1.00126
2	-1.5595812	-1.5617	1.00136
3	-1.3546211	-1.3566	1.00146
4	-1.1704091	-1.1723	1.00162
5	-1.0057168	-1.0075	1.00177
6	-0.8592746	-0.86087	1.00186
7	-0.7297888	-0.73125	1.00200
8	-0.6159592	-0.61729	1.00216
9	-0.5164938	-0.51770	1.00234
10	-0.4301231	-0.43120	1.00250
11	-0.3556114	-0.35657	1.00270
12	-0.2917683	-0.29261	1.00288
13	-0.2374567	-0.23820	1.00313
14	-0.1916004	-0.19224	1.00334
15	-0.1531898	-0.15374	1.00359
16	-0.1212858	-0.12176	1.00391
17	-9.5022481(-02)	-9.5438(-02)	1.00437
18	-7.3608067(-02)	-7.3940(-02)	1.00451
19	-5.6325397(-02)	-5.6599(-02)	1.00486
20	-4.2530440(-02)	-4.2754(-02)	1.00526
21	-3.1650256(-02)	-3.1831(-02)	1.00571
22	-2.3180032(-02)	-2.3323(-02)	1.00617
23	-1.6679434(-02)	-1.6791(-02)	1.00669
24	-1.1768423(-02)	-1.1854(-02)	1.00727
25	-8.1226859(-03)	-8.1873(-03)	1.00795
26	-5.4687973(-03)	-5.5165(-03)	1.00872
27	-3.5792655(-03)	-3.6136(-03)	1.00959
28	-2.2675456(-03)	-2.2916(-03)	1.01061
29	-1.3831324(-03)	-1.3995(-03)	1.01183
30	-8.0680818(-04)	-8.1747(-04)	1.01321
31	-4.4611287(-04)	-4.5276(-04)	1.01490
32	-2.3077899(-04)	-2.3503(-04)	1.01842
33	-9.4777816(-05)	-1.1252(-04)	1.18720
34		-4.8564(-05)	
35		-1.8262(-05)	
36		-5.6648(-06)	
37		-1.3175(-06)	
38		-1.9247(-07)	
39		-1.1215(-08)	
40		-4.1916(-11)	

TABLE VIII Vibrational levels for the 0_g^- electronic state of the $^{23}\text{Na}_2$ molecule as obtained with a fixed step RK4 method, Stwalley *et al.* (57) results and the corresponding ratio. Levels 34-40 were not found by the RK4 method due to the precision limited to fourth order.

Index	Stwalley <i>et al.</i> (cm ⁻¹)	VSCA (cm ⁻¹)	Ratio
1	-1.7887	-1.7864488	1.00126
2	-1.5617	-1.5595638	1.00137
3	-1.3566	-1.3546072	1.00147
4	-1.1723	-1.1703990	1.00162
5	-1.0075	-1.0057071	1.00178
6	-0.86087	-0.8592631	1.00187
7	-0.73125	-0.7297908	1.00200
8	-0.61729	-0.6159534	1.00202
9	-0.51770	-0.5164882	1.00235
10	-0.43120	-0.4301217	1.00251
11	-0.35657	-0.3556148	1.00269
12	-0.29261	-0.2917693	1.00288
13	-0.23820	-0.2374560	1.00313
14	-0.19224	-0.1916002	1.00334
15	-0.15374	-0.1531893	1.00359
16	-0.12176	-0.1212854	1.00391
17	-9.5438(-02)	-9.5022588(-02)	1.00437
18	-7.3940(-02)	-7.3608452(-02)	1.00450
19	-5.6599(-02)	-5.6325744(-02)	1.00485
20	-4.2754(-02)	-4.2530867(-02)	1.00525
21	-3.1831(-02)	-3.1650591(-02)	1.00570
22	-2.3323(-02)	-2.3180420(-02)	1.00615
23	-1.6791(-02)	-1.6679756(-02)	1.00667
24	-1.1854(-02)	-1.1768655(-02)	1.00725
25	-8.1873(-03)	-8.1228816(-03)	1.00793
26	-5.5165(-03)	-5.4689541(-03)	1.00869
27	-3.6136(-03)	-3.5793742(-03)	1.00956
28	-2.2916(-03)	-2.2676168(-03)	1.01058
29	-1.3995(-03)	-1.3831806(-03)	1.01180
30	-8.1747(-04)	-8.0683859(-04)	1.01318
31	-4.5276(-04)	-4.4613249(-04)	1.01486
32	-2.3503(-04)	-2.3110168(-04)	1.01700
33	-1.1252(-04)	-1.1035443(-04)	1.01962
34	-4.8564(-05)	-4.7468345(-05)	1.02308
35	-1.8262(-05)	-1.7767388(-05)	1.02784
36	-5.6648(-06)	-5.4747950(-06)	1.03471
37	-1.3175(-06)	-1.2597092(-06)	1.04588
38	-1.9247(-07)	-1.2716754(-07)	1.51352
39	-1.1215(-08)		
40	-4.1916(-11)		

TABLE IX Vibrational levels for the 0_g^- electronic state of the $^{23}\text{Na}_2$ molecule as obtained with Stwalley *et al.* results, the VSCA method and the corresponding ratio. Levels 38, 39 and 40 of Stwalley *et al.* (57) are extrapolated with LeRoy and Bernstein (36) semi-classical formulae.

The parameter $C(1_u)$ is such that:

$$\cos^{-1}\left(\frac{1+270X^3}{\sqrt{(1+63X^2)^3}}\right), \text{ and } Q = \frac{1+63X^2}{9}. \quad \lim_{r \rightarrow +\infty} V(r) \rightarrow -\frac{C_3(1_u)}{r^3} \quad (33)$$

Index	RK4 (cm ⁻¹)	Stwalley <i>et al.</i> (cm ⁻¹)	Ratio
1	0.1319536	0.13212	1.00126
2	9.0057392(-02)	9.0192(-02)	1.00149
3	5.9472159(-02)	5.9574(-02)	1.00171
4	3.7821597(-02)	3.7896(-02)	1.00197
5	2.3027828(-02)	2.3080(-02)	1.00227
6	1.3324091(-02)	1.3359(-02)	1.00262
7	7.2562182(-03)	7.2787(-03)	1.00310
8	3.6714971(-03)	3.6849(-03)	1.00365
9	1.6950002(-03)	1.7024(-03)	1.00437
10	6.9533077(-04)	6.9904(-04)	1.00533
11	2.4102039(-04)	2.4492(-04)	1.01618
12		6.8430(-05)	
13		1.3446(-05)	
14		1.4122(-06)	
15		3.8739(-08)	
16		1.2735(-12)	

TABLE X Vibrational levels for the 1_u electronic state of the $^{23}\text{Na}_2$ molecule as obtained with the RK4 method, Stwalley *et al.* results and the corresponding ratio. RK4 found only 11 levels and levels 15 and 16 of Stwalley *et al.* are found by extrapolation.

Index	Stwalley <i>et al.</i> (cm ⁻¹)	VSCA (cm ⁻¹)	Ratio
1	0.13212	0.13244150	1.00243
2	9.0192(-02)	9.07598688(-02)	1.00630
3	5.9574(-02)	6.01645742(-02)	1.00991
4	3.7896(-02)	3.83982868(-02)	1.01325
5	2.3080(-02)	2.34584275(-02)	1.01640
6	1.3359(-02)	1.36187753(-02)	1.01944
7	7.2787(-03)	7.44243743(-03)	1.02250
8	3.6849(-03)	3.77999552(-03)	1.02581
9	1.7024(-03)	1.75281307(-03)	1.02961
10	6.9904(-04)	7.23013793(-04)	1.03430
11	2.4492(-04)	2.54856605(-04)	1.04057
12	6.8430(-05)	7.18249908(-05)	1.04961
13	1.3446(-05)	1.43120199(-05)	1.06441
14	1.4122(-06)	1.53931042(-06)	1.09001
15	3.8739(-08)	4.66022073(-09)	
16	1.2735(-12)		

TABLE XI Vibrational levels for the 1_u electronic state of the $^{23}\text{Na}_2$ molecule as obtained by Stwalley *et al.*, the VSCA and the corresponding ratio. A new 15th level is obtained with the VSCA method.

Identification of the large r limit yields to the result: $C_3(1_u) = C(1_u)(\sqrt{7}-2)/9$. We have used in the calculations below $C_3(1_u) = 1.383 \text{ Hartrees} \cdot a_0^3$ like Stwalley *et al.* The parameter $\Delta = 1.56512 \cdot 10^{-4} \text{ Rydbergs}$ is the same as for the 0_g^- state.

Table IV displays the results we obtain with the RK4 method that cannot find more than 11 levels due to accuracy limitations.

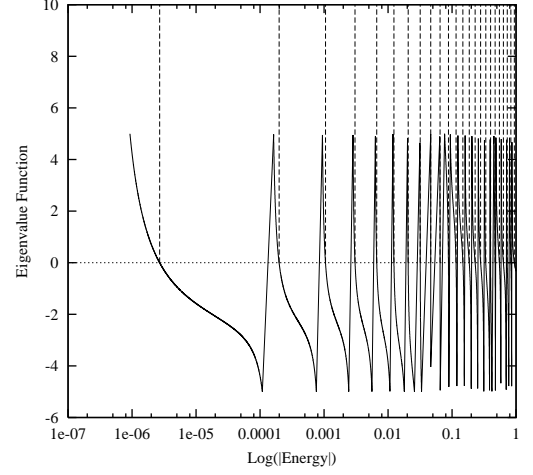


FIG. 8 Behavior of the eigenvalue function $F(E)$ with energy on a semi-log scale for the Trost *et al.* (60) Lennard-Jones molecule. The vertical lines indicate the eigenvalue position. Energies are in potential depth ϵ units.

The next results for the 1_u electronic state of the $^{23}\text{Na}_2$ molecule are obtained with the VSCA method as shown in table V. We find an additional 15-th level in contrast to Stwalley *et al.* who found fourteen and extrapolated the last two levels.

The corresponding graph of the eigenvalue function is displayed in Fig. 6 below.

B. Lennard-Jones molecules

We apply our methodology to the Lennard-Jones case. Our results are compared to the results obtained by Trost *et al.* (60). We start with the levels obtained with the RK4 method. The energy unit is ϵ the absolute value of potential well depth. The Asymmetric Lennard-Jones potential (ALJ) is given by:

$$V(r) = \frac{C_1}{r^\beta} - \frac{C_2}{r^\alpha} \quad (34)$$

It depends on C_1 and C_2 that yield an equilibrium distance at $r = r_e$ and a potential depth $-\epsilon$. In order to compare with the appropriate literature, Trost *et al.* (60) use rather the general parameterisation:

$$C_1 = \frac{\epsilon}{(\beta - \alpha)} \alpha r_e^\beta, \quad C_2 = \frac{\epsilon}{(\beta - \alpha)} \beta r_e^\alpha \quad (35)$$

It is scaled in such a way that the energy is expressed in units of the potential well depth $-\epsilon$. When $\alpha = 6$, $\beta = 12$ we obtain $r_e = \sqrt[6]{\frac{2C_1}{C_2}}$ and $\epsilon = \frac{C_2^2}{4C_1}$. and the

radial distance is in $\frac{a_0}{\sqrt{B}}$ where B is a reduced scaled mass given by $B = 2\mu\epsilon r_e^2$. Numerically Trost *et al.* use $B = 10^4$ which is the order of magnitude encountered in long-range molecules within the framework of their system of units. The potential energy in these units is displayed in Fig. 7. The RK4 methods yields the results displayed in Table VI.

The accuracy limitation of the RK4 results in losing the uppermost level 24. Thus we move on to the results obtained with the superior VSCA method. All levels are obtained with the VSCA and the agreement with Trost *et al.* results is perfect as witnessed by the ratio values of Table 6. The eigenvalue function obtained with the VSCA method as a function of energy is displayed in Fig. 8.

V. TEST OF BOHR CORRESPONDANCE PRINCIPLE

LeRoy and Bernstein (36) used a WKB approximation to derive a semi-classical formula (SCF) for the distribution of vibrational levels near the dissociation limit of diatomic molecules. If the long-range interatomic potential is of the form $D - C_n/r^n$ their formula allows the determination of the dissociation energy D as well as the tail of the potential (n and C_n) from the experimental energies of the highest vibrational levels. Furthermore, this analysis opens the possibility of testing directly Bohr Correspondence Principle (BCP) that states the agreement between semi-classical and quantum results improves for larger quantum numbers.

We consider the rotationless ($L=0$) 0_g^- and the 1_u electronic states of the $^{23}\text{Na}_2$ molecule correlating asymptotically to the atomic $^2P_{3/2}$ and $^2S_{1/2}$ states. The interaction between the atoms is represented by the Movre-Pichler (42) potential that behaves as $-1/r^3$ as $r \rightarrow +\infty$ and we use the same parameters as those of Stwalley *et al.* (57). The Asymmetric Lennard-Jones potential (ALJ) $C_1 r^{-\beta} - C_2 r^{-\alpha}$ is also considered in the highly unsymmetric case $C_2 \gg C_1$ (we tackle here the case $\beta = 12$ and $\alpha = 6$, therefore we have asymptotically $-1/r^6$) and the Trost *et al.* (60) case. Both potentials are tailored to the study of Long-range molecules.

The determination of the vibrational spectra of these very tenuous molecules is extremely subtle especially for the highest levels which play an important role in photoassociation spectroscopy. Special care is needed in order to diagonalise the Hamiltonian without losing accuracy for all energies including those close to the dissociation limit.

The magnitudes of potential energy, distance and mass values in this kind of molecules stand several orders of magnitude above or below what is encountered in ordinary short-range molecules. For instance the typical

intramolecular potential well depth at the equilibrium distance of about 100 a_0 (Bohrs), is a fraction of a cm^{-1} while the reduced mass is several 10,000 electron masses as observed in the Johnson case previously. All these extreme values require special numerical techniques in order to avoid roundoffs, divergences, numerical instability and ill-conditioning during processing.

Accuracy and its control being of paramount importance in this work, the CFM (29) is an excellent candidate because it bypasses the calculation of the eigenfunctions. This avoids losing accuracy associated with the numerical calculation specially with rapidly oscillating wave functions of highly excited states close to the dissociation limit.

The semi-classical approximation has been already discussed in the literature (6; 60). Here we refer to the original LeRoy and Bernstein formulation.

The next section is a discussion of the the Semi-classical analysis as formulated by LeRoy and Bernstein with its implications. We present further the results we obtain for the vibrational levels of the $^{23}\text{Na}_2$ molecule 0_g^- and 1_u electronic states. We present an additional validation of the method with the ALJ molecular potential.

A. Semi-classical analysis

The derivation of the LeRoy and Bernstein (36) SCF is based on the WKB condition for the eigenvalues of a potential $V(r)$:

$$v + 1/2 = \frac{\sqrt{2\mu}}{\pi\hbar} \int_{R_1(v)}^{R_2(v)} \sqrt{E(v) - V(R)} dR \quad (36)$$

where μ is the reduced mass, $E(v)$ is the energy of the level indexed by v and $R_1(v), R_2(v)$ are the the corresponding classical turning points.

Near the dissociation limit, one considers $E(v)$ as a continuous function of v and by differentiation of eq. (36) one obtains:

$$\frac{dv}{dE(v)} = \frac{\sqrt{\mu/2}}{\pi\hbar} \int_{R_1(v)}^{R_2(v)} \frac{1}{\sqrt{E(v) - V(R)}} dR \quad (37)$$

Using the asymptotic expression of $V(r) = D - C_n/r^n$ and changing the variable of integration to $y = R_2(v)/R$, we obtain:

$$\frac{dv}{dE(v)} = \frac{\sqrt{\mu/2}}{\pi\hbar} \int_1^{R_2(v)/R_1(v)} y^{-2} (y^n - 1)^{-1/2} dy \quad (38)$$

This integral can be expressed in terms of incomplete Euler Beta functions we use to check the accuracy and validate the results. LeRoy and Bernstein (36) SCF is derived by taking the limit $R_2(v)/R_1(v) \rightarrow +\infty$ which leads to:

$$\frac{dE(v)}{dv} = K_n [D - E(v)]^{\frac{(n+2)}{2n}} \quad (39)$$

Index	RK4	Trost <i>et al.</i>	Ratio
1	-0.9410450	-0.9410460	1.000001
2	-0.8299980	-0.8300020	1.000005
3	-0.7276400	-0.7276457	1.000008
4	-0.6336860	-0.6336930	1.000011
5	-0.5478430	-0.5478520	1.000017
6	-0.4698130	-0.4698229	1.000021
7	-0.3992870	-0.3992968	1.000025
8	-0.3359470	-0.3359561	1.000027
9	-0.2794670	-0.2794734	1.000023
10	-0.2295070	-0.2295117	1.000021
11	-0.1857220	-0.1857237	1.000009
12	-0.1477510	-0.1477514	1.000003
13	-0.1152270	-0.1152259	0.999990
14	-8.776970(-02)	-8.7766914(-02)	0.999968
15	-6.498640(-02)	-6.4982730(-02)	0.999944
16	-4.647400(-02)	-4.6469911(-02)	0.999912
17	-3.181750(-02)	-3.1813309(-02)	0.999868
18	-2.059000(-02)	-2.0586161(-02)	0.999814
19	-1.235370(-02)	-1.2350373(-02)	0.999731
20	-6.659580(-03)	-6.6570240(-03)	0.999616
21	-3.048890(-03)	-3.0471360(-03)	0.999425
22	-1.053690(-03)	-1.0527480(-03)	0.999106
23	-1.645210(-04)	-1.9834000(-04)	1.205560
24		-2.6970000(-06)	

TABLE XII Quantum levels of a Lennard-Jones molecule in ϵ units, the depth of the potential well as obtained by the RK4 method, Trost *et al.* and the corresponding ratio. Only the last 24th level was missed by the RK4 method.

Index	VSCA	Trost <i>et al.</i>	Ratio
1	-0.9410443	-0.9410460	1.000002
2	-0.8299963	-0.8300020	1.000007
3	-0.7276415	-0.7276457	1.000006
4	-0.6336915	-0.6336930	1.000002
5	-0.5478480	-0.5478520	1.000007
6	-0.4698206	-0.4698229	1.000005
7	-0.3992947	-0.3992968	1.000005
8	-0.3359533	-0.3359561	1.000008
9	-0.2794718	-0.2794734	1.000005
10	-0.2295109	-0.2295117	1.000003
11	-0.1857222	-0.1857237	1.000008
12	-0.1477498	-0.1477514	1.000010
13	-0.1152247	-0.1152259	1.000010
14	-8.7766358(-02)	-8.7766914(-02)	1.000006
15	-6.4982534(-02)	-6.4982730(-02)	1.000003
16	-4.6469838(-02)	-4.6469911(-02)	1.000002
17	-3.1813146(-02)	-3.1813309(-02)	1.000005
18	-2.0585953(-02)	-2.0586161(-02)	1.000010
19	-1.2350173(-02)	-1.2350373(-02)	1.000016
20	-6.6568735(-03)	-6.6570240(-03)	1.000023
21	-3.0470500(-03)	-3.0471360(-03)	1.000028
22	-1.0526883(-03)	-1.0527480(-03)	1.000057
23	-1.9832170(-04)	-1.9834000(-04)	1.000092
24	-2.6957891(-06)	-2.6970000(-06)	1.000449

TABLE XIII Quantum levels of a Lennard-Jones molecule in ϵ units, the depth of the potential well as obtained by the VSCA method, Trost *et al.* and the corresponding ratio.

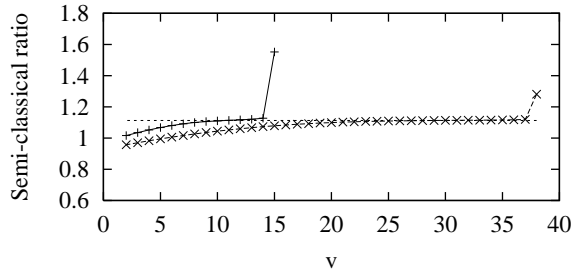


FIG. 9 Approach of the semi-classical limit for the 0_g^- and 1_u (upper curve) electronic states of the $^{23}\text{Na}_2$ molecule with the vibrational quantum number.

where K_n is a constant we calculate below for $n=3$ and $n=6$. Integrating the above equation yields:

$$[D - E(v)]^{1/2-1/n} = \frac{(n+2)}{2n} K_n (v_{max} - v + v_D) \quad (40)$$

where v_{max} is the uppermost vibrational level index and v_D is generally not an integer that depends on interactions having shorter range (36; 57).

Taking the origin of energies at the dissociation limit and following Gao (20), we define a length scale with:

$$\beta_n = \left(\frac{2\mu C_n}{\hbar^2} \right)^{\frac{1}{(n-2)}} \quad (41)$$

This length should be larger than any length scale encountered in the system. In the case $n=3$, one defines a dimensionless bound-state energy by the scaling:

$$\epsilon_s(v) = \frac{1}{4} \frac{E(v)}{(\hbar^2/2\mu)(1/\beta_3)^2} \quad (42)$$

With the use of eq. (40) this leads to:

$$[-\epsilon_s(v)]^{1/6} = \frac{[\Gamma(1/3)]^3}{2^{5/3} 3^{1/2} \pi} (v_{max} - v + v_D) \quad (43)$$

This implies that the spacing between two scaled neighbouring vibrational levels taken to power (1/6) is a universal constant given by $\frac{[\Gamma(1/3)]^3}{2^{5/3} 3^{1/2} \pi}$ numerically equal to 1.11292.

In the Lennard-Jones and the Trost *et al.* cases ($n=6$), the scaled bound-state energy takes the form:

$$\epsilon_s(v) = \frac{1}{16} \frac{E(v)}{(\hbar^2/2\mu)(1/\beta_6)^2} \quad (44)$$

Proceeding like the previous case, eq. (40) leads to:

$$[-\epsilon_s(v)]^{1/3} = \frac{[\Gamma(1/3)]^3}{2^{5/3}\pi} (v_{max} - v + v_D) \quad (45)$$

In this case, the spacing between two scaled neighbouring vibrational levels taken to power (1/3) is given by $\frac{[\Gamma(1/3)]^3}{2^{5/3}\pi}$ numerically equal to 1.92763. Thus, one has to determine the vibrational levels and examine the limit of $E(v)$ as v increases.

B. Test with the $^{23}\text{Na}_2$ molecule

We apply the CFM to the calculation of the vibrational energy levels of a diatomic molecule where the

interaction between the atoms is given by the Movre and Pichler potential (26; 42).

After scaling all energies with a factor E_0 (usually cm^{-1}) and all distances with a typical length L_0 the potential coefficients in the RSE are transformed in a way such that the functional form of the potential is preserved.

The eigenvalue function $F(E)$ depicted in fig. 10 shows that the $\tan(E)$ shape is observed again indicating that the CFM is able to perform accurately as previously despite the extreme sensitivity of this problem.

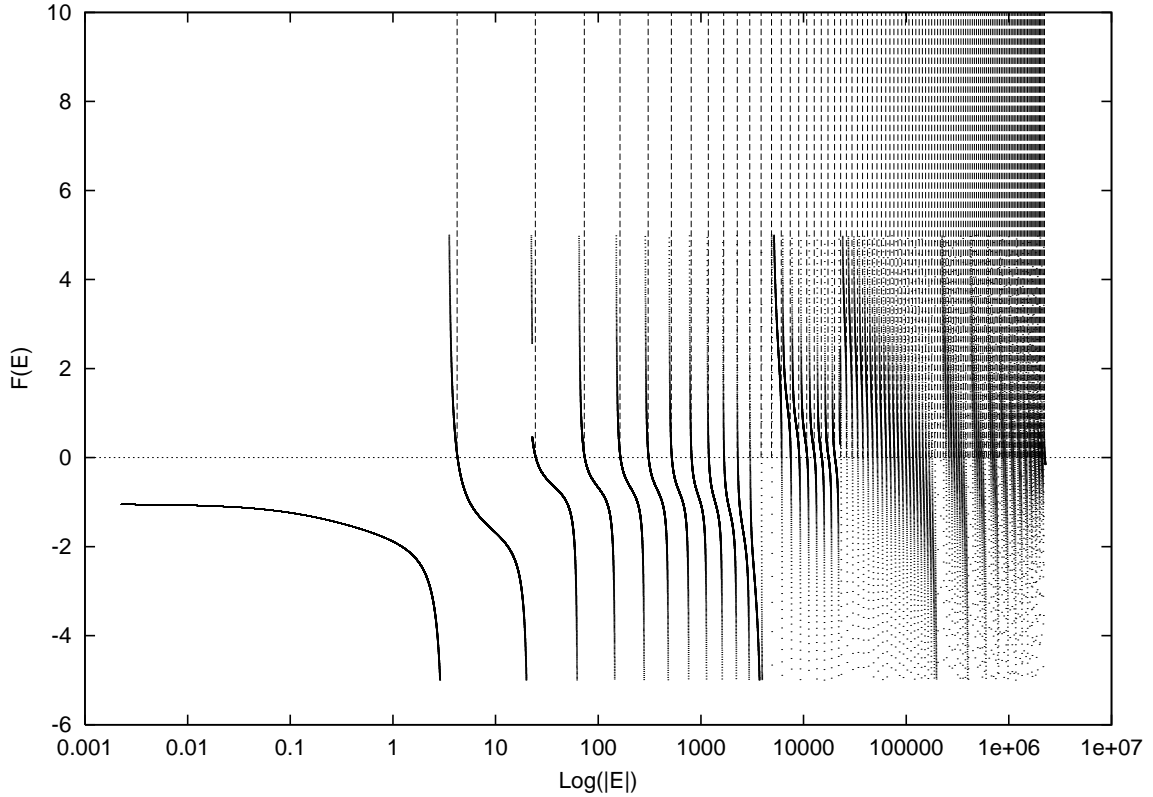


FIG. 10 Behavior of the eigenvalue function $F(E)$ with energy on a semi-log scale for the Trost *et al.* (60) ALJ ($C_1 = 1, C_2 = 3000$) molecule. The vertical lines indicate the eigenvalue position. Energies are in potential depth ϵ units.

The integration of the RSE is performed with the VSCA method (35). This method is superior to fixed step methods and is based on a series expansion of the

potential and the corresponding solution to an order such that a required tolerance criterion is met. Ideally, the series coefficients are determined analytically to any

order, otherwise loss of accuracy occurs leading quickly to numerical uncertainties.

This method is powerful and flexible enough to find all the sought levels plus additional levels not detected before by Stwalley *et al.* (57). It should be noted that the last three levels given by Stwalley *et al.* (57) were extrapolated and not calculated. The agreement between the rest of our own calculated levels and those of Stwalley *et al.* is quite good.

We find all sought levels plus an additional level that was not detected before. The agreement between our calculated levels and those of Stwalley *et al.* (57) turns out to be very good.

The semi-classical analysis is displayed in Fig. 9. It shows clearly that the sequence of Vibrational levels approaches the semi-classical limit 1.11292. The departure from this limit at the uppermost side of the spectrum is stronger for the 1_u than for the 0_g^- state. A crossover region is spanned by the semi-classical limit and appears to be narrower for the 1_u than for the 0_g^- case.

C. Test with Lennard-Jones molecules

We apply our methodology to the Asymmetric Lennard-Jones case (ALJ) as considered by Trost *et al.* (60). After obtaining good agreement between the CFM eigenvalues and Trost *et al.*'s we display the results of the semi-classical analysis in Fig. 6. The sequence of neighbouring levels approaches the theoretical limit 1.92763. The departure from this limit at the uppermost side of the spectrum is stronger for the Trost case than for the ($C_1 = 1, C_2 = 3000$) ALJ case and the width of the crossover region is almost zero in the Trost *et al.* case.

Gao (20) applied this analysis to sequences of neighbouring levels with his own calculated levels and claimed that BCP breaks down for all quantum systems in which the asymptotic interaction is of the form $1/r^n$ with $n > 2$.

Additionally Gao found that the agreement between his calculated levels and the SCF is better around the middle of the vibrational spectra contrary to Stwalley *et al.*'s (57) and our work.

Fig. 2 clearly shows that the semi-classical limit is reached as we increase the quantum number for the 0_g^- and 1_u states of the $^{23}\text{Na}_2$ molecule. The departure is obtained with the levels we obtained at the high end of the spectra with the VSCA method based on the CFM. The crossover region is wider in the 0_g^- case and the departure is smaller.

On the other hand, Fig. 3 pertaining to the Lennard-Jones ($V(r) \sim -1/r^6$) case shows that the crossover region is quite narrow for the ALJ as well as the Trost *et al.* case in comparison with the $^{23}\text{Na}_2$ case. The departure is also stronger in the Trost case. Additional

work is needed in order to tie the width of the crossover region to the asymptotic character of the potential.

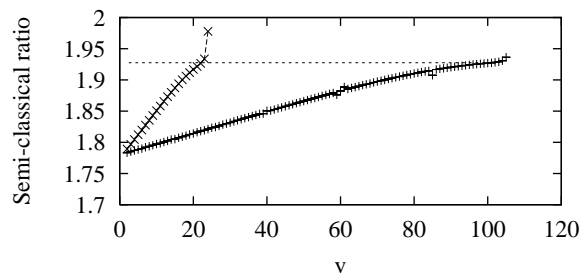


FIG. 11 Approach of the semi-classical limit for the ALJ ($C_1 = 1, C_2 = 3000$) potential as well as the Trost *et al.* (60) model (upper curve) with the vibrational quantum number.

VI. EXCHANGE: LOCAL AND NON-LOCAL

Calculations of cross sections for photoionisation require the resolution of the integro-differential equations satisfied by the radial parts of the free electron wavefunctions. Very often a simplifying approximation is made through replacement of the exchange operator by a central equivalent exchange potential (Furness and McCarthy (19), Bransden and Noble (7)). While this is probably satisfactory for electrons with energies of a few eV and more it may cause problems near to threshold. Furthermore, to interpret the new generation of experiments using polarized electrons the proper inclusion of exchange may well be important. There exists a means of exact solution of the equation for the radial wavefunction including static and static-exchange terms (the diagonal parts of the direct potential and the exchange operator) and a polarisation potential. This is the Distorted Wave Polarised Orbital (DWPO) method of McDowell *et al.* (39) which was developed for Distorted Wave Born calculations of excitation of Hydrogen (McDowell *et al.* (40)) and of Helium (56) and replaces the integro-differential equation by coupled differential equations. In both cases, only an s-state of the atom is considered and the central potentials are expressed in analytical form.

The phaseshift and the wavefunction in the asymptotic region were determined by use of the analytic second order JWKB solution (Burgess (10)). The solutions are started by means of series expansions at the origin and continued by Numerov (43) integration: the form of series corresponding to the regular solution is imposed by taking a power $r^{l'+1}$ at the origin in the l' partial wave. For small k the choice of integration step and changeover point is delicate, since convergence of the series requires small r whereas the Numerov integration becomes unstable (picking up some of the irregular solution) if it is started at too small a radius.

Accuracy in evaluating the scattering phaseshift produced in electron atom collisions is demanded in

order to estimate reliably the cross section (49). In (e, 2e) (62) collision type experiments, triple Differential Cross Sections (TDCS) for electron impact ionization of an atom or ion, estimated within the Distorted Wave Born Approximation (DWBA), are required.

Computational difficulties such as instabilities, lack of accuracy or convergence slow-down arise in solving the corresponding Schrödinger equation. The latter has to respect Pauli exclusion principle stating that the wave function of the incident electron be anti-symmetric with the wave functions of the electrons in the target atom or molecule. In the Hartree-Fock formulation, this requirement leads to the presence of non local terms in the resulting coupled differential equations satisfied by the radial parts of the free electron wavefunctions (49; 62). The non-local kernel of the integro-differential type equation originating from the exchange operator is often simplified and a central LEE potential is used or some decoupling procedure is employed (23). A review of the different methods to treat this problem on the basis of the Lippman-Schwinger equation is given by Rawitscher *et al.* (49). Furness and McCarthy (19) and Bransden and Noble (7) cover the DWBA aspects.

Using a local exchange potential approximation is probably satisfactory for electrons with energies of a few eV and more, however it may cause problems near to threshold. On the other hand, the interpretation of experiments using polarized electrons, requires proper account for exchange. In addition, it is worthwhile to develop a version of the DWBA (62) including non-local exchange and applicable to heavy atom targets. This stems from the fact, the successful Converged Close Coupling (CCC) approach of Bray (8) becomes increasingly difficult to apply as target complexity increases.

The Distorted Wave Polarised Orbital (DWPO) method is a means for extracting the exact solution of

the radial wave equation with static, static-exchange terms (the diagonal parts of the direct potential and the exchange operator) and some polarisation potential. It has been developed by McDowell *et al* (39) for DWBA calculations for the ionization of Hydrogen (McDowell *et al* (40)) and of Helium (56). It replaces the integro-differential equation by coupled differential equations. Only an s-state of the Hydrogen or Helium atoms is considered and the central potentials are expressed in analytical form.

The phaseshift and the wavefunction in the asymptotic region are determined by use of the analytic second order JWKB solution (Burgess (10)). If the energy of the free electron is k^2 Ry, the integro-differential equation can be rewritten in terms of the variable kr but the value of the radius out to which exchange and the short-range part of the static potential remain significant, is determined by the extent of the electron cloud of the atom. For small k , the second order JWKB solution is valid only at radii very much larger than that of the asymptotic zone where exchange and short-range potentials are negligible.

A. The integro-differential equation

We consider the impact of a free electron of energy k^2 Ry on a one-electron atomic system of nuclear charge Z in a $1s$ atomic state of energy E_{10} Ry with a radial wavefunction $R_{10}(r) = 2Z^{3/2}r \exp(-Zr)$. For a free electron with angular momentum quantum numbers l', m' , if we include only on-diagonal potentials and exchange operators and replace the neglected off-diagonal coupling potentials by a polarisation potential $V_{pol}(r)$, its radial wavefunction $F_{l'}(k, r)$ satisfies the integro-differential equation:

$$\left[\frac{\partial^2}{\partial r^2} - \frac{l'(l'+1)}{r^2} + k^2 + V_{1s}(r) + V_{pol}(r) + W_{l'}(r) \right] F_{l'}(k, r) = 0 \quad (46)$$

where:

$$V_{1s}(r) = \frac{2Z}{r} - \frac{2}{r} \int_0^r |R_{10}(r')|^2 dr' - \int_r^\infty \frac{2}{r'} |R_{10}(r')|^2 dr' \quad (47)$$

and:

$$W_{l'}(r)F_{l'}(k, r) = (-1)^{S+1}R_{10}(r) \left\{ [E_{10} - k^2] \delta_{l',0} \int_0^\infty R_{10}(r')F_{l'}(k, r')dr' - \frac{2}{r} \int_0^r R_{10}(r')F_{l'}(k, r')dr' - \int_r^\infty \frac{2}{r'} R_{10}(r')F_{l'}(k, r')dr' \right\} \quad (48)$$

This integro-differential equation can be transformed into the following system of coupled differential equations, which is the starting point for McDowell *et al* (39; 40):

$$\begin{aligned} & \frac{\partial^2}{\partial r^2} F_{l'}(k, r) - \left[\frac{l'(l'+1)}{r^2} - \mathcal{V}_{1s}(r) \right] F_{l'}(k, r) \\ & + (-1)^S R_{10}(r) \left[\frac{2}{r} \frac{1}{2l'+1} \right] G_{l'}(k, r) = (-1)^{S+1} R_{10}(r) \delta_{l',0} A(k) \\ & \frac{\partial^2}{\partial r^2} G_{l'}(k, r) - \frac{l'(l'+1)}{r^2} G_{l'}(k, r) + \frac{2l'+1}{r} R_{10}(r) F_{l'}(k, r) = 0 \end{aligned} \quad (49)$$

where

$$A(k) = [k^2 - E_{10}] \int_0^\infty R_{10}(r') F_{l'}(k, r') dr' \quad (50)$$

is a term appearing for the special case of zero orbital momentum ($l' = 0$). $\delta_{l',0}$ is the Kronecker delta and

$$\mathcal{V}_{1s}(r) = k^2 + V_{1s}(r) + V_{pol}(r) \quad (51)$$

Our aim is to solve this system subject to the boundary conditions (39; 40) for the Hartree functions:

$$\begin{aligned} F_{l'}(k, r) & \xrightarrow{r \rightarrow 0} 0 & G_{l'}(k, r) & \xrightarrow{r \rightarrow 0} 0 \\ F_{l'}(k, r) & \xrightarrow{r \rightarrow \infty} a_{l'}(k) \{s_{l'}(kr) - \tan[\delta_{l'}(k)] c_{l'}(kr)\} & G_{l'}(k, r) & \xrightarrow{r \rightarrow \infty} 0 \end{aligned} \quad (52)$$

where $a_{l'}(k)$ is a normalisation factor, $\delta_{l'}(k)$ is the phaseshift for specific $\{k, l'\}$ and $s_{l'}(\rho)$ and $c_{l'}(\rho)$ are respectively:

- ρ multiplied spherical Bessel and Neumann functions when $Z = 1$ (so that $\mathcal{V}_{1s}(r)$ is a short range potential falling off faster than r^{-1} as r tends to infinity);

- regular and irregular Coulomb wavefunctions when $Z > 1$ (so that $\mathcal{V}_{1s}(r)$ is a long range potential behaving like $(Z-1)r^{-1}$ when r tends to infinity).

In the more general case of an ion with a frozen core and an outer shell of electrons in $\{n, l\}$ states of radial wavefunction $R_{nl}(r)$, and a free electron in the state $\{k, l'\}$ we have a larger set of coupled equations:

$$\begin{aligned} & \frac{\partial^2}{\partial r^2} F_{l'}(k, r) - \left[\frac{l'(l'+1)}{r^2} - \mathcal{V}_{nl}(r) \right] F_{l'}(k, r) \\ & - (-1)^S R_{nl}(r) \frac{2}{r} \sum_{\lambda} J_{l,l',\lambda} G_{l'}^\lambda(k, r) = (-1)^{S+1} R_{nl}(r) \delta_{l,l'} A_{nl,l'}(k) \\ & \frac{\partial^2}{\partial r^2} G_{l'}^\lambda(k, r) - \frac{\lambda(\lambda+1)}{r^2} G_{l'}^\lambda(k, r) + \frac{2\lambda+1}{r} R_{nl}(r) F_{l'}(k, r) = 0 \end{aligned} \quad (53)$$

where:

$$\begin{aligned} & \mathcal{V}_{nl}(r) = k^2 - V_{nl}(r) \\ & -2 \sum_{\lambda} I_{l,l',\lambda} \left\{ \int_0^r \frac{r'^\lambda}{r^{\lambda+1}} |R_{nl}(r')|^2 dr' + \int_r^\infty \frac{r'^\lambda}{r'^{\lambda+1}} |R_{nl}(r')|^2 dr' \right\} + V_{pol}(r) \end{aligned} \quad (54)$$

and:

$$A_{nl,\nu'}(k) = [k^2 - E_{nl}] \int_0^\infty R_{nl}(r') F_{\nu'}(k, r') dr' \quad (55)$$

These equations are subject to the boundary conditions, for all possible λ values:

$$\begin{aligned} F_{\nu'}(k, r) &\xrightarrow[r \rightarrow 0]{} 0 & G_{\nu'}^\lambda(k, r) &\xrightarrow[r \rightarrow 0]{} 0 \\ F_{\nu'}(k, r) &\xrightarrow[r \rightarrow \infty]{} a_{\nu'}(k) \{s_{\nu'}(kr) - \tan[\delta_{\nu'}(k)] c_{\nu'}(kr)\} & G_{\nu'}^\lambda(k, r) &\xrightarrow[r \rightarrow \infty]{} 0 \end{aligned} \quad (56)$$

$I_{l,\nu',\lambda}$ and $J_{l,\nu',\lambda}$ are angular integrals which depend on the number of electrons in the ion outer shell and the angular momentum coupling scheme. $V_{nl}(r)$ is a central potential for attraction of an electron by the core and E_{nl} is the total energy of the outer shell electrons. This is not applicable to hydrogenic ions as the degeneracy of the energy in l makes it essential to include channel coupling potentials. We will not consider it further here except to note that $J_{l,\nu',\lambda}$ imposes the triangular rule $|l - l'| \leq \lambda \leq l + l'$ and $l + l' + \lambda$ even. This gives an idea of the number of different $G_{\nu'}^\lambda$ present and the extent of the problem we ultimately wish to solve, in the case of more complex atoms.

B. The CFM for solving the DWPO equations

In order to facilitate the presentation it is convenient to use f_1 in place of $F_{\nu'}$ and f_2 in place of $G_{\nu'}$ so as to rewrite the coupled equation system (2) as a special case of the more general system:

$$\begin{aligned} f_1''(r) + V_{11}(r)f_1(r) + V_{12}(r)f_2(r) &= \delta_{\nu',0}A(k)W_1(r) \\ f_2''(r) + V_{22}(r)f_2(r) + V_{21}(r)f_1(r) &= \delta_{\nu',0}A(k)W_2(r) \end{aligned} \quad (57)$$

with

$$\begin{aligned} V_{11}(r) &= \mathcal{V}_{1s}(r) - \frac{l'(l'+1)}{r^2}, & V_{12}(r) &= (-1)^S R_{10}(r) \left[\frac{2}{r} \frac{1}{(2l'+1)} \right], \\ V_{21}(r) &= \frac{(2l'+1)}{r} R_{10}(r), & V_{22}(r) &= -\frac{l'(l'+1)}{r^2}, \\ W_1(r) &= (-1)^{S+1} R_{10}(r), & W_2(r) &= 0 \end{aligned} \quad (58)$$

We can construct the general solution of the above equations as (see Kobeissi and Fakhreddine (32)):

$$\begin{aligned} f_1(r) &= f_1(r_0)\alpha_{11}(r) + f_1'(r_0)\beta_{11}(r) + f_2(r_0)\alpha_{12}(r) + f_2'(r_0)\beta_{12}(r) + \delta_{\nu',0}A(k)\sigma_1(r) \\ f_2(r) &= f_1(r_0)\alpha_{21}(r) + f_1'(r_0)\beta_{21}(r) + f_2(r_0)\alpha_{22}(r) + f_2'(r_0)\beta_{22}(r) + \delta_{\nu',0}A(k)\sigma_2(r) \end{aligned} \quad (59)$$

where $\{\alpha_{1j}(r), \alpha_{2j}(r)\}$ and $\{\beta_{1j}(r), \beta_{2j}(r)\}$ are two different pairs of independent solutions of the homogeneous system:

$$g_1''(r) + V_{11}(r)g_1(r) + V_{12}(r)g_2(r) = 0 \quad (60)$$

$$g_2''(r) + V_{22}(r)g_2(r) + V_{21}(r)g_1(r) = 0 \quad (61)$$

satisfying the initial conditions at an arbitrary point $r = r_0$

$$\alpha_{ij}(r_0) = \beta_{ij}'(r_0) = \delta_{ij}, \quad \alpha_{ij}'(r_0) = \beta_{ij}(r_0) = 0$$

and $\{\sigma_1(r), \sigma_2(r)\}$ is a particular solution of the inhomogeneous system:

$$h_1''(r) + V_{11}(r)h_1(r) + V_{12}(r)h_2(r) = W_1(r) \quad (62)$$

$$h_2''(r) + V_{22}(r)h_2(r) + V_{21}(r)h_1(r) = W_2(r) \quad (63)$$

satisfying the initial conditions at $r = r_0$

$$\sigma_i(r_0) = \sigma_i'(r_0) = 0 \quad (64)$$

The general solution in matrix form is written as:

$$Y(r) = \alpha(r)Y(r_0) + \beta(r)Y'(r_0) + \delta_{\nu',0}A(k)\sigma(r) \quad (65)$$

with

$$Y(r) = \begin{pmatrix} f_1(r) \\ f_2(r) \end{pmatrix}, \quad \alpha(r) = \begin{pmatrix} \alpha_{11}(r) & \alpha_{12}(r) \\ \alpha_{21}(r) & \alpha_{22}(r) \end{pmatrix}, \quad \beta(r) = \begin{pmatrix} \beta_{11}(r) & \beta_{12}(r) \\ \beta_{21}(r) & \beta_{22}(r) \end{pmatrix} \quad (66)$$

Each column of the (2x2) matrices $\alpha(r)$ and $\beta(r)$ is a particular solution of 61 with initial values given by 62. The column matrix: $\sigma(r) = (\sigma_1(r), \sigma_2(r))$ is a particular solution of 63 with initial condition given by 64. Using the boundary conditions 56 imposes: $\alpha(0)Y(r_0) + \beta(0)Y'(r_0) + \delta_{l',0}A(k)\sigma(0) = 0$, which leads to $\beta^{-1}(0)\alpha(0)Y(r_0) + Y'(r_0) + \delta_{l',0}A(k)\beta^{-1}(0)\sigma(0) = 0$ where $\beta^{-1}(r)$ is the inverse of the matrix $\beta(r)$.

Thus, the constant matrices at point $r = r_0$, $Y'(r_0)$ and $Y(r_0)$ are related by:

$$Y'(r_0) = Y(r_0)\Lambda + \delta_{l',0}A(k)\lambda, \quad (67)$$

where the matrices Λ and λ are given by:

$$\Lambda = -\beta^{-1}(0)\alpha(0), \quad \lambda = -\beta^{-1}(0)\sigma(0) \quad (68)$$

Substituting back into 65 we then get:

$$Y(r) = \varphi(r)Y(r_0) + \delta_{l',0}A(k)\gamma(r) \quad (69)$$

the functions $\varphi(r)$ and $\gamma(r)$ are related to the particular solutions $\alpha(r), \beta(r)$ and $\sigma(r)$ by:

$$\varphi(r) = \alpha(r) + \beta(r)\Lambda, \quad \gamma(r) = \beta(r)\lambda + \sigma(r) \quad (70)$$

We notice again that $\varphi(r) = (\phi_1(r), \phi_2(r))$ and $\gamma(r) = (\gamma_1(r), \gamma_2(r))$ are particular solutions of system (8) since they are linear combinations of $\alpha(r)$ and $\beta(r)$.

The initial values at the arbitrarily chosen starting point $r = r_0$ are:

$$\varphi(r_0) = I, \varphi'(r_0) = \Lambda, \gamma(r_0) = 0, \gamma'(r_0) = \lambda \quad (71)$$

where I is the unit matrix. The solution constructed from $\varphi(r)$ and $\gamma(r)$ is a particular solution of the coupled equations (8) for which the functions $\{f_1(r), f_2(r)\}$ are regular at the origin.

C. Phaseshift calculation

From the first of boundary conditions we can determine the phaseshift δ_l from:

$$\tan \delta_{l'} = \lim_{r \rightarrow \infty} Q(r), \quad \text{where:} \quad (72)$$

$$Q(r) = -\frac{f_1'(r)s_{l'}(kr) - f_1(r)ks_{l'}'(kr)}{f_1'(r)c_{l'}(kr) - f_1(r)kc_{l'}'(kr)}$$

We follow Kobeissi *et al* (35) in using the recursion relations for $s_{l'}(\rho)$ and $c_{l'}(\rho)$:

$$Q(r) = \frac{\begin{matrix} Z = 1 : \\ \left[f_1'(r) - \frac{(l'+1)}{r} f_1(r) \right] s_{l'}(kr) + k f_1(r) s_{l'+1}(kr) \\ \left[f_1'(r) - \frac{(l'+1)}{r} f_1(r) \right] c_{l'}(kr) + k f_1(r) c_{l'+1}(kr) \end{matrix}}{\begin{matrix} Z > 1 : \\ \left[f_1'(r) + \left\{ \frac{(Z-1)}{k(l'+1)} - \frac{(l'+1)}{r} \right\} f_1(r) \right] s_{l'}(kr) + \sqrt{k^2 + \frac{(Z-1)^2}{(l'+1)^2}} f_1(r) s_{l'+1}(kr) \\ \left[f_1'(r) + \left\{ \frac{(Z-1)}{k(l'+1)} - \frac{(l'+1)}{r} \right\} f_1(r) \right] c_{l'}(kr) + \sqrt{k^2 + \frac{(Z-1)^2}{(l'+1)^2}} f_1(r) c_{l'+1}(kr) \end{matrix}} \quad (73)$$

The function $Q(r)$ can be obtained for any radius r . We calculate it at large r values and examine its behaviour. When it tends to a constant limit, we consider that the asymptotic region has been reached and the phaseshift is determined modulo 2π .

Numerically, the phaseshift is actually calculated with

the following steps:

1. An arbitrary point r_0 is chosen as the origin to proceed with the integration.
2. The canonical functions $\alpha(r)$, $\beta(r)$ and $\sigma(r)$ are computed for $r < r_0$: Eqs 61 and 63 are integrated

starting at r_0 with $\alpha(r)$, $\beta(r)$ and $\sigma(r)$ initialised with 62 and 64. The matrices Λ and λ are deduced. Progressing toward the origin $r = 0$, the integration is stopped when the matrices Λ and λ attain stable values. Numerically, this is done by monitoring the values of their determinants.

3. The computation of Λ and λ serves to calculate the other canonical functions $\varphi(r)$ and $\gamma(r)$ and consequently estimate A_1 and A_2 .
4. Repeating the computation with $r \geq r_0$ allows to calculate the ancillary functions $f_1(r)$, $f'_1(r)$ and $Q(r)$ (relations 72 and 73). The calculation is stopped when $Q(r)$ attains a stable value corresponding to $\tan \delta$. The stability of the phase-shift value is attained when the ratio $|Q(r_{p+1}) - Q(r_p)|/|Q(r_{p+1}) + Q(r_p)| \leq \epsilon_S$, where $[r_p, r_{p+1}]$ is the interval obtained after p integration steps and ϵ_S is termed the stability error.

The phaseshift overall error (desired error or tolerance) depends on both ϵ_T and ϵ_S as well as computer/compiler arithmetic, roundoff errors and intermediate algorithmic/numerical operations. We estimate it through a comparison with analytical or other available results (such as asymptotic or at special points).

For small k the outward Numerov integration of the regular solution can get out of control if it picks up a tiny fraction of the irregular solution, because of ill-

conditioning due to round-off errors. An alternative is to modify the potential by introducing a hard core: $\mathcal{V}_{nl}(r)$ is set artificially to infinity for $r < r_s$, where r_s is the starting point of the integration and retains its original form for $r > r_s$.

As mentioned by Bayliss (4) *et al*, this method gives results sensitive to the point in the classically forbidden region at which the integration is started. If the starting point is too small some solutions become unstable; if it is too large for the initial conditions used, the solution is inaccurate. In the CFM, the solutions $\alpha(r)$, $\beta(r)$ and $\sigma(r)$ initially generated are in fact linear combinations of the regular and irregular solutions of the coupled equations and by taking the linear combinations $\varphi(r)$ and $\gamma(r)$ we eliminate from them the irregular solution.

D. Phaseshift accuracy and comparison to the S-IEM

We apply the present method to the case of the collision of a low-energy electron with atomic hydrogen, *i.e.* generating the wavefunctions needed for DWBA calculations of electron impact ionization of atomic hydrogen. In this case the static potential is given by:

$$V_{1s}(r) = -2 \left(1 + \frac{1}{r} \right) \exp(-2r) \quad (74)$$

Like McDowell and collaborators, we use a Callaway-Temkin polarisation potential (see Drachman and Temkin (12)) of the form:

$$V_{pol}(r) = -\frac{9}{2r^4} \left[1 - e^{-2r} \left(1 + 2r + 2r^2 + \frac{4}{3}r^3 + \frac{2}{3}r^4 + \frac{4}{27}r^5 \right) \right] \quad (75)$$

To integrate the coupled equation system, preference is given in the present work to the VSCA method described above. The latter method was shown by Kobeissi *et al* (15; 30; 33) to be highly accurate in the case of both single and coupled differential equations. It requires potentials to be expressed in analytical form. Numerical potentials can generally be fitted by piecewise analytical or polynomial functions such as cubic splines. The integration can be safely taken out to a very large radius,

where $\mathcal{V}_{1s}(r)$ assumes its asymptotic form and the phase-shift determined. We refer to this method as the CFM Exact Exchange (CFMEE).

In order to further gauge the reliability of our results, we performed a series of calculations varying the stability error ϵ_S and the truncation error ϵ_T in order to test the accuracy and convergence speed of our method. The tests are displayed in the tables below for the singlet case:

Recently, Rawitscher *et al.* (49) obtained very accurate results for the phaseshift at $l' = 0$ for momentum $k = 0.2/a_0$ in the absence of any polarization potential but with rigorous inclusion of the Fock exchange term. They obtained the phaseshifts and scattering lengths in the singlet and triplet states. The method they use, the

S-IEM (Spectral Integral Equation Method), is based on partitioning the integration interval $[0, r_{max}]$ into a fixed number of partitions expressing the integration kernel with a set of four different functions. This transforms the problem into a block tridiagonal matrix system built from sets of 4x4 block matrices corresponding each to a

TABLE XIV Singlet ($S = 0, l' = 0$) phaseshifts for e-H scattering versus momentum as the stability error is decreased while truncation error ϵ_T is fixed at 10^{-14} (upper sub-table) and as the truncation error is decreased with a fixed stability error $\epsilon_S = 10^{-14}$ (lower sub-table)

k	Stability error ϵ_S					
	10^{-4}	10^{-6}	10^{-8}	10^{-10}	10^{-12}	10^{-14}
0.1	2.54421122	2.53027301	2.5274412	2.52744125	2.52744125	2.52744125
0.2	2.06575195	2.03935101	2.03407088	2.03407088	2.03407088	2.03407088
0.3	1.70757716	1.67206099	1.66518977	1.66518968	1.66518968	1.66518968
0.4	1.42957123	1.3914665	1.38497592	1.38497592	1.38497592	1.38497592
0.5	1.2095031	1.17365026	1.16825708	1.16825708	1.16825708	1.16825708
0.6	1.03735556	1.00552357	1.00072357	1.00072404	1.00072404	1.00072404
0.7	0.90616322	0.87811171	0.87375939	0.87376024	0.87376024	0.87376024
0.8	0.80734542	0.78365856	0.77961723	0.77961723	0.77961723	0.77961723
0.9	0.75274001	0.75420532	0.71342049	0.71342026	0.71342027	0.71342027
1.0	0.69239713	0.7010382	0.6701203	0.6701203	0.6701203	0.6701203

k	Truncation error ϵ_T					
	10^{-4}	10^{-6}	10^{-8}	10^{-10}	10^{-12}	10^{-14}
0.1	3.00127274	3.0307537	2.52412523	2.52463171	2.52558189	2.5274412
0.2	2.82900282	2.88186498	2.02681296	2.02795407	2.03007799	2.03407088
0.3	2.65292424	1.65536145	1.65611743	1.65755527	1.66025047	1.66518977
0.4	2.4734271	1.37484701	1.37567631	1.37717447	1.37993599	1.38497592
0.5	1.15828993	1.15870411	1.15948866	1.16092162	1.16354419	1.16825708
0.6	2.14501974	0.9920774	0.99279684	0.9941118	0.99649203	1.00072357
0.7	0.86558783	0.8658675	0.86653892	0.86774235	0.86992432	0.87375939
0.8	1.8745865	0.77331792	0.7738408	0.77481281	0.77655005	0.77961723
0.9	1.72900321	0.70870253	0.70910062	0.70982718	0.71113237	0.71342049
1.0	1.60803611	0.66656396	0.66686498	0.66741118	0.6684008	0.6701203

given partition (49).

The phaseshift expressed in the form $k/\tan(\delta)$ versus momentum k is displayed for the singlet and the triplet in Fig. 5. Our results (crosses) fall exactly on top of the continuous curves for the singlet and the triplet obtained by Rawitscher *et al.* (49) with the S-IEM. Whenever, either of the curves cross the horizontal axis, the phaseshift

value is $\pi/2$ modulo (π) and $\tan(\delta)$ is singular. The CFM method like the S-IEM, had no particular difficulty (instability or slowing down) in reproducing the singularity and the phaseshifts were obtained as described in section 5.1, for arbitrarily small values of the momentum k ($k \geq 10^{-8}$ in $1/a_0$ units).

The rate of convergence as a function of stability error ϵ_S of the CFM result for the triplet phaseshift at $k = 0.2/a_0$ is displayed in table XV along with the S-IEM result. It is remarkable to observe that as the stability error is decreased, we obtain steady convergence toward the S-IEM result. If we consider, in that case, the S-IEM result as exact, we can infer that the overall desired error (tolerance) behaves as $\sim \epsilon_S^{0.45}$, implying that ϵ_S is a good indicator of accuracy despite its deterioration across intermediate arithmetic operations.

The scattering length a for the electron-hydrogen atom scattering is based on the low momentum expansion of the scattering phaseshift:

$$k \cot \delta = -1/a + r_e k^2 + O(k^3) \quad (76)$$

where r_e the effective range (49). The left-hand side of the above expression is calculated for two very small values of the momentum k differing by a factor of two and the values of a and r_e are solved for (49). This procedure is repeated for decreasing values of k and stability error ϵ_S until the numerical value of the result is obtained to a given number of significant figures. In table XVI, we display the results of the CFM and S-IEM for the singlet case. The agreement between the S-IEM result for the scattering length 8.100312397 and the corresponding CFM result (8.100307932) is excellent.

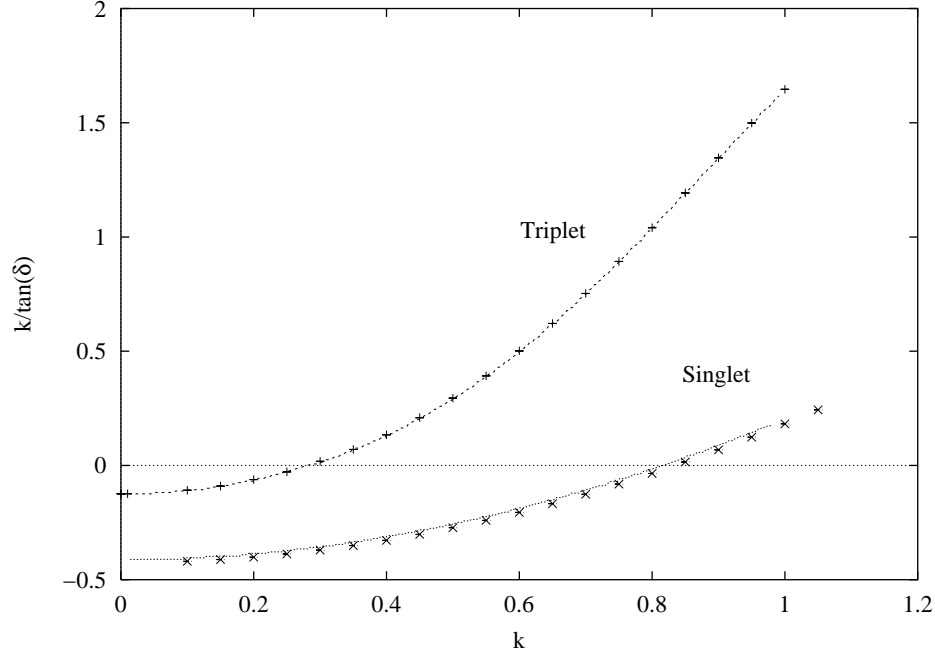


FIG. 12 Singlet and Triplet $l' = 0$, CFMEE results (crosses) values of $k/\tan(\delta)$ versus incident momentum k in $1/a_0$ units and comparison to Rawitscher *et al.* (continuous lines). The smallest value used for k is 10^{-8} .

TABLE XV Triplet phaseshift accuracy as the stability error is decreased at $k = 0.2/a_0$. S-IEM is Rawitscher *et al.* Spectral Integral Equation Method

Stability error ϵ_S	δ
10^{-4}	1.8927821
10^{-5}	1.8773093
10^{-6}	1.8724465
10^{-7}	1.8708870
10^{-8}	1.8703880
10^{-9}	1.8702301
10^{-12}	1.8701771
S-IEM	1.8701579

TABLE XVI Singlet scattering length versus momentum as the stability error is decreased. S-IEM is Rawitscher *et al.* Spectral Integral Equation Method

k	Stability error ϵ_S		
	10^{-4}	10^{-6}	10^{-8}
10^{-2}	8.058030140	8.104593677	8.109676748
10^{-3}	8.081922310	8.098359718	8.100205405
10^{-4}	8.093862531	8.099570349	8.100235983
10^{-5}	8.098414768	8.100045256	8.100281954
10^{-6}	8.100073345	8.100226775	8.100299303
10^{-8}	8.100305162	8.100305163	8.100307932
S-IEM	8.100312397		

The CFM result is obtained for a value of momentum $k = 10^{-8}/a_0$ and stability error $\epsilon_S = 10^{-8}$, whereas the S-IEM result was obtained with a value of momentum $k = 10^{-5}/a_0$, and maximum integration range $r_{max} \sim 50$ with approximately 1000 mesh points.

Finally we display in table XVII the result for the triplet scattering length as momentum k decreases steadily toward $k = 10^{-8}/a_0$.

TABLE XVII Triplet scattering length (with 10^{-8} stability error) as momentum decreases and comparison to the S-IEM result. Note the faster convergence than the singlet case.

k	a
10^{-2}	2.3497331
10^{-3}	2.3493995
10^{-4}	2.3493961
10^{-5}	2.3493961
10^{-6}	2.3493961
10^{-7}	2.3493961
10^{-8}	2.3493961
S-IEM	2.3493961

Roche *et al.* (53) developed, recently, an exact exchange method, within the DWBA, for the evaluation of high and low energy electron impact ionisation experiments on Hydrogen and Lithium, with presence of polarisation. In the table below, we compare our results (CFMEE) to theirs for the singlet and triplet s-wave phaseshifts at high energies. The polarisation used is of

the form: $V_{pol}(r) = -\frac{\alpha}{2r^4}$.

TABLE XVIII Singlet s-wave phaseshifts with polarization $V_{pol}(r) = -\frac{\alpha}{2r^4}$ and comparison to the CFMEE method.

Energy in eV	CFMEE	Roche <i>et al.</i> (53)
14.6	-1.46166	-1.46084
15.0	-1.4720848	-1.47127
15.6	-1.48717379	-1.48642
17.6	-1.53373849	-1.53297
20.0	-1.58264557	-1.51896
25.0	-1.66616627	-1.66483
30.0	-1.73100847	-1.73061

TABLE XIX Triplet s-wave phaseshifts with polarization $V_{pol}(r) = -\frac{\alpha}{2r^4}$ and comparison to the CFMEE method.

Energy in eV	CFMEE	Roche <i>et al.</i> (53)
14.6	-1.45993029	-1.43966
15.0	-1.46697595	-1.44676
15.6	-1.47691298	-1.45683
17.6	-1.50572363	-1.48681
20.0	-1.53328328	-1.51529
25.0	-1.57639125	-1.56060
30.0	-1.60975092	-1.59548

The remarkable agreement shows that our method performs well at high energies and presence of polarisation, with methods using exact exchange instead of local exchange. Our work has also shown that a distorted wave code, with exact treatment of exchange and Numerov integration, breaks down with appearance of numerical instabilities at energies below about 5 eV. Codes with LEE potentials give poor results for low partial waves at energies below 15 eV.

VII. ONE-DIMENSIONAL POTENTIAL PROBLEMS

In the last section before the conclusion, we apply the CFM to a couple of 1D potentials to illustrate once again its capabilities beyond the focus of this work mainly concerned with the 3D case.

The archetypical 1D problem is the infinite square well potential of width w defined by:

$$V(x) = 0, \quad 0 < x < w, \quad V(0) = \infty, \quad V(w) = \infty,$$

the eigenvalues are given by: $E_n = \frac{\hbar^2}{2m_p} \left(\frac{n\pi}{w}\right)^2, n = 1, 2, \dots$ with m_p is the particle mass (not necessarily an electron as generally assumed).

In order to conform with the CFM general framework, one transforms the closed finite interval $[0, w]$ to the open infinite interval $[0, \infty[$.

It is interesting to note that while, in general, the CFM maps an arbitrary potential (infinite interval) over the infinite square well potential (finite interval), this problem might be viewed exactly as the reverse mapping.

With the use of the transformation $r = \frac{x}{(w-x)}$ the Schrödinger equation is transformed into:

$$-\frac{\hbar^2}{2m_p} \frac{d^2\psi(x)}{dx^2} = E\psi(x), \quad 0 < x < w \quad (77)$$

with the boundary conditions: $\psi(0) = 0, \psi(w) = 0$.

The Schrödinger equation defined over the interval $0 < r < \infty$ acquires a first-order derivative term becoming:

$$-\frac{\hbar^2}{2m_p} \left[\frac{(1+r)^4}{w^4} \frac{d^2\psi(r)}{dr^2} + \frac{2(1+r)^3}{w^2} \frac{d\psi(r)}{dr} \right] = E\psi(r), \quad (78)$$

The VSCA algorithm derived earlier for the standard Schrödinger equation must be altered into (using units such that $\hbar = 1, m_p = 1$):

$$(n+2)(n+1)C_{n+2}^{(p)} = -2 \sum_{m=0}^n (m+1)a_{n-m}^{(p)}C_{m+1}^{(p)} - 2Ew^2 \sum_{m=0}^n b_{n-m}^{(p)}C_m^{(p)} \quad (79)$$

where the $a_m^{(p)}, b_m^{(p)}$ are, respectively, the coefficients of the series expansion of $\frac{1}{(1+r)}$ and $\frac{1}{(1+r)^4}$ over the interval $I_p = [r_p, r_{p+1}]$.

The results are displayed in the table below proving once again the remarkable versatility of the CFM method.

After proving the success of the CFM over a finite interval we move on to the standard application over the usual infinite interval $[0, \infty[$.

Double-minimum Potential Well (DPW) problems are interesting to solve as they arise in many areas of Atomic, Molecular and even Solid State physics. They are encountered in highly excited Rydberg states of atoms in crossed electric and magnetic fields and in certain molecular potential curves. When two-dimensional electron layers (such as in semiconducting heterostructures) are placed in perpendicular electric and magnetic fields, a potential well with two minima,

CFM	Index	Exact	Ratio
0.004 440 783	1	0.004 444 444	0.9992
0.017 917 823	2	0.017 777 776	1.0078
0.040 324 728	3	0.039 999 999	1.0081
0.071 671 344	4	0.071 111 105	1.0078
0.111 964 293	5	0.111 111 104	1.0076
0.161 208 108	6	0.159 999 996	1.0075
0.219 427 973	7	0.217 777 774	1.0075
0.286 566 615	8	0.284 444 422	1.0074
0.362 612 218	9	0.359 999 985	1.0072
0.447 584 212	10	0.444 444 418	1.0070
0.541 484 714	11	0.537 777 781	1.0068
0.644 318 163	12	0.639 999 986	1.0067
0.756 076 396	13	0.751 111 090	1.0066
0.876 762 569	14	0.871 111 095	1.0064
1.006 386 52	15	0.999 999 94	1.0063

TABLE XX Quantum levels of the infinite square well potential given by the CFM along with exact results and the ratio of the CFM to the exact eigenvalue. The well width w is chosen in a way such that the eigenvalue is 1 when the number of levels is 15.

for the electronic motion normal to the surface, arises.

A DPW can be symmetric or asymmetric and one has to adapt in each case the appropriate boundary condition imposed by the CFM (see Appendix on matching and boundary conditions).

An interesting DPW is the symmetric Double Gaussian potential investigated by Hamilton and Light (22). It is given by:

$$V(r) = -D[\exp(-\Omega(r - r_a)^2) + \exp(-\Omega(r + r_a)^2)]$$

The values of the parameters: D, Ω, r_a are respectively: 12.0, 0.1, 5.0 in standard a.u such that $\hbar = 1, \mu = m_e = 1$.

The results shown for all the 24 levels in table XXI prove unambiguously the accuracy of the CFM method and its high level of competitiveness with respect to the somehow sophisticated method used by Hamilton and Light (22) based on Distributed Gaussian Basis sets inspired from Quantum Chemistry Techniques.

Johnson has studied an asymmetric DWP consisting of the sum of a Morse and a Gaussian resulting in the expression:

$$V(r) = D[1 - \exp(-B(r - r_a))]^2 + A \exp(-C(r - r_b)^2)$$

The values of the parameters A, B, C, D, r_a, r_b are (following Johnson (25)) in ($\text{cm}^{-1}, \text{\AA}$ system of units) are: $10^4 \text{ cm}^{-1}, 1.54 \text{\AA}^{-1}, 200.0 \text{\AA}^{-2}, 31250.0 \text{ cm}^{-1}, 1.5 \text{\AA}, 1.6 \text{\AA}$ respectively.

Eigenvalues for the asymmetric double minimum potential problem are given in table XXII and a compar-

CFM	Index	Hamilton and Light
-11.250 418 469	0	-11.245 199 313
-9.779 202 594	2	-9.773 496 902
-8.387 701 732	4	-8.381 307 510
-7.079 415 041	6	-7.072 039 562
-5.858 805 474	8	-5.849 958 02
-4.732 231 858	10	-4.720 829 36
-3.709 907 559	12	-3.694 518 38
-2.807 436 691	14	-2.798 251 92
-2.022 064 904	16	-2.089 661 3
-1.293 090 067	18	-1.462 202 9
-0.601 483 056	20	-0.771 081
-0.067 153 689	22	-0.177 181
-11.250 421 409	1	-11.245 199 313
-9.779 225 834	3	-9.773 496 902
-8.387 719 137	5	-8.381 307 491
-7.079 412 929	7	-7.072 038 846
-5.858 811 221	9	-5.849 940 0
-4.732 171 001	11	-4.720 509 6
-3.709 113 861	13	-3.690 475 6
-2.801 628 760	15	-2.763 219 7
-2.000 566 637	17	-1.924 577
-1.255 332 005	19	-1.149 254
-0.561 216 170	21	-0.457 88
-0.045 810 537	23	-0.003 41

TABLE XXI Computed eigenvalues for the symmetric double Gaussian well potential. The even index results are shown separately from the odd index since they correspond to different symmetries. The numbers at left are the levels computed with the CFM; on the right the levels obtained by Hamilton and Light (22). Note the deterioration of accuracy of the Hamilton and Light results as the index increases because of the approach of the continuum.

ison between Johnson's (25) results and the CFM are displayed below.

VIII. CONCLUSIONS

In this review, we have shown that the CFM is a very powerful and accurate method that is able to solve a large variety of quantum problems such as:

- Energy levels for regular and singular potentials (radial case)
- Pseudo-potential estimation (parametric potential) from spectroscopic data
- Accurate Phase shift evaluation for regular and singular potentials
- Test of the Bohr Correspondence Principle

Index	Johnson	CFM
0	1302.500	1302.498 972
1	3205.307	3205.303 782
2	4227.339	4227.336 543
3	5144.251	5144.243 754
4	6064.241	6064.225 881
5	7092.679	7092.664 815
6	7614.622	7614.603 506
7	8911.545	8911.513 342
8	9095.696	9095.679 497
9	10208.350	10208.318 142
10	10869.289	10869.255 077
11	11482.475	11482.457 956
12	12353.799	12353.766 422
13	12972.473	12972.453 117
14	13690.455	13690.436 602
15	14435.350	14435.321 044

TABLE XXII Eigenvalues in cm^{-1} of the Johnson asymmetric DWP consisting of the sum of a Morse and a Gaussian potentials $V(r) = D[1 - \exp(-B(r - r_a))]^2 + A \exp(-C(r - r_b)^2)$, with $A = 10^4 \text{cm}^{-1}$, $B = 1.54 \text{\AA}^{-1}$, $C = 200.0 \text{\AA}^{-2}$, $D = 31250.0 \text{cm}^{-1}$, $r_a = 1.5 \text{\AA}$, $r_b = 1.6 \text{\AA}$. Johnson (25) results are compared to the CFM.

- Vibrational energy levels of Cold Molecules and application to the $^{23}\text{Na}_2$ molecule in the 0_g^- and 1_u electronic states. The Lennard-Jones molecule case is also studied.
- Local and Non-Local Exchange problems.
- Energy levels for regular and singular potentials (general 1D case)

Its mathematics is quite subtle since it enables one to find the Vibrational spectra of tenuous molecules where energies and distances are so remote from the ordinary short-range molecules case that special techniques should be developed in order to avoid numerical instabilities and uncertainties.

The CFM has been tested successfully in Long-range and Short-range potentials for Atomic and Molecular states and gives accurate results for bound and free states (29; 31; 35). The tunable accuracy of our method allows to evaluate eigenvalues close to the ground state as well as close to highly excited states near the continuum limit to a large number of digits without any extrapolation.

The CFM compares favorably with many different sophisticated techniques such as those developed, for instance (to cite a few), by Raptis *et al.* (46; 47), Johnson (25), Hamilton *et al.* (22) and Rawitscher *et al.* (49).

The CFM approach remains the same despite the wide variability of the mentioned problems.

The VSCA integration method used gives the right number of all the levels and the variation of the eigenvalue function $F(E)$ definitely determines the total number of levels. Generally it requires performing analytically Taylor series expansion to any order of an arbitrary potential function that might require the combination of numerical, symbolic manipulation, functional fitting and analytic function continuation techniques (see refs (16; 17)). Despite these challenges, the results of the VSCA are rewarding.

The use of the RK4 and the VSCA methods jointly paves the way to a precise comparative evaluation of the accuracy of the spectra obtained. In practice, the RK4 method can be used in optimisation problems whereas the VSCA is more adapted to the direct evaluation of the spectra.

Since the CFM bypasses the calculation of the eigenfunctions, it avoids losing accuracy associated with the numerical calculation specially with rapidly oscillating wave functions of highly excited states. This is specially needed in the study of the sensitive problem of determining the vibrational spectra of cold molecules.

We did not consider molecular rotation, nevertheless the CFM is adapted to solve accurately Ro-Vibrational problems as well as any RSE diagonalisation problem (see for instance ref. (31)).

Regarding spin dependent scattering problems we applied the CFM to local and non-local exchange integrating exactly the coupled equations originating from integro-differential equations. We benchmarked and tested our integration method at extremely small energies for momentum $k \geq 10^{-8}$ and found that it performs again very well against stability error ϵ_S and truncation error ϵ_T . Our results were validated with a highly accurate method, the recently developed S-IEM (49). The results we find (phaseshifts and scattering lengths) agree with the S-IEM results for the singlet, triplet cases for an arbitrarily small value of momentum k ($k \geq 10^{-8}$).

In conclusion, the (single channel and multichannel) CFM enables one to tackle precisely weakly bound states in atoms and (simple and cold) molecules as well as low-energy scattering of atoms and molecules and can be extended straightforwardly to Bose-Einstein condensation problems (60).

Acknowledgements: This work is dedicated to the memory of Hafez Kobeissi (1936-1998), our past teacher (CT and KF) and colleague who laid the foundations of the CFM. Part of this work was performed on the IDRIS (Cray and IBM Clusters) machines at the CNRS (Orsay).

We would like to acknowledge helpful correspondence with Jeff Cash (Imperial College), Ronald Friedman (Purdue), Bengt Fornberg (Caltech) and John W. Wilkins (Ohio state).

APPENDIX

Atomic and other units

In atomic and molecular physics, it is convenient to use the elementary charge e , as the unit of charge, and the electron mass m_e as the unit of mass (although for some purposes the proton mass, m_p , or the unified mass unit amu, is more convenient). Electrostatic forces and energies in atoms are proportional to $e^2/4\pi\epsilon_0$, which has dimensions ML^3T^{-2} , and another quantity that appears all over in quantum physics is \hbar which has dimensions ML^2T^{-1} ; so it is convenient to choose units of length and time such that $4\pi\epsilon_0 = 1$ and $\hbar = 1$.

The atomic unit of length is then (by dimensional analysis alone)

$$a_B = \frac{e^2}{m_e(e^2/4\pi\epsilon_0)} \quad (80)$$

This is called the Bohr radius, or simply the bohr (0.529 Å), because in the "Bohr model" the radius of the smallest orbit for an electron circling a fixed proton is $(1 + m_e/m_p)a_B$. In the full quantum theory the particles do not follow an orbit, but the expectation value of the electron-proton distance in the Hydrogen ground state is exactly $(1 + m_e/m_p)a_B$.

The atomic unit of energy is the Hartree (27.2 eV) given by:

$$E_h = \frac{e^2}{4\pi\epsilon_0} \frac{1}{a_B} = \left(\frac{e^2}{4\pi\epsilon_0}\right)^2 \frac{m_e}{\hbar^2} \quad (81)$$

The unit of time is \hbar/E_h .

The Hartree is twice the ground state energy of the Hydrogen atom $\frac{1}{2}(1 + m_e/m_p)^{-1}E_h$ equal to the Rydberg (13.6 eV). In atomic and molecular spectroscopy, one uses rather the cm^{-1} an energy corresponding to a wavelength of 1cm or sometimes a frequency unit, the Hz. We refer the reader to the table below giving the conversion factors between the different energies.

	J	eV	Hz	cm^{-1}
1 J	= 1	6.24151.10 ¹⁸	1.50919.10 ³³	5.03411.10 ²²
1 eV	= 1.60219.10 ⁻¹⁹	1	2.41797.10 ¹⁴	8.06547.10 ³
1 Hz	= 6.62619.10 ⁻³⁴	4.13570.10 ⁻¹⁵	1	3.33564.10 ⁻¹¹
1 cm^{-1}	= 1.96648.10 ⁻²³	1.23935.10 ⁻⁴	2.99792.10 ¹⁰	1

Matching and boundary conditions

The CFM is based on the extraction of the eigenvalues from the zeroes of the eigenvalue function $F(E)$ defined from the saturation of the left ($r \rightarrow 0$) and right ($r \rightarrow +\infty$) functions $l_-(E)$ and $l_+(E)$ given by the ratios of the canonical functions $\alpha(r)$ and $\beta(r)$. This was described previously in the case the boundary conditions are $y(0) = y(\infty) = 0$. In the general case we write:

$$\begin{aligned} y(r) &= y(r_0)\alpha(E; r) + y'(r_0)\beta(E; r) \\ y'(r) &= y(r_0)\alpha'(E; r) + y'(r_0)\beta'(E; r) \end{aligned} \quad (82)$$

The canonical functions satisfy the conditions:

$$\alpha(E; r_0) = 1, \alpha'(E; r_0) = 0, \beta(E; r_0) = 0, \beta'(E; r_0) = 1 \quad (83)$$

Let us rewrite the system 82 at the two boundaries $r = 0$:

$$\begin{aligned} y(0) &= y(r_0)\alpha(E; 0) + y'(r_0)\beta(E; 0) \\ y'(0) &= y(r_0)\alpha'(E; 0) + y'(r_0)\beta'(E; 0) \end{aligned} \quad (84)$$

and at $r = \infty$:

$$\begin{aligned} y(\infty) &= y(r_0)\alpha(E; \infty) + y'(r_0)\beta(E; \infty) \\ y'(\infty) &= y(r_0)\alpha'(E; \infty) + y'(r_0)\beta'(E; \infty) \end{aligned} \quad (85)$$

Extracting from above the left and right ratios:

$$\begin{aligned} \left[\frac{y'(r_0)}{y(r_0)} \right]_- &= \frac{\alpha(E; 0)y'(0) - \alpha'(E; 0)y(0)}{\beta'(E; 0)y(0) - \beta(E; 0)y'(0)} \\ \left[\frac{y'(r_0)}{y(r_0)} \right]_+ &= \frac{\alpha(E; \infty)y'(\infty) - \alpha'(E; \infty)y(\infty)}{\beta'(E; \infty)y(\infty) - \beta(E; \infty)y'(\infty)} \end{aligned} \quad (86)$$

we can tackle several types of boundary conditions providing below the energy functions $l_-(E)$ and $l_+(E)$ that determine the eigenvalue function:

$$F(E) = l_+(E) - l_-(E) = \left[\frac{y'(r_0)}{y(r_0)} \right]_+ - \left[\frac{y'(r_0)}{y(r_0)} \right]_- \quad (87)$$

Some of the boundary conditions are, for instance:

1. Standard (Dirichlet) case:

The boundary conditions $y(0) = y(\infty) = 0$ yield:

$$\begin{aligned} l_-(E) &= \lim_{r \rightarrow 0} -\frac{\alpha(E; r)}{\beta(E; r)} \\ l_+(E) &= \lim_{r \rightarrow +\infty} -\frac{\alpha(E; r)}{\beta(E; r)} \end{aligned} \quad (88)$$

2. Derivative asymmetric case type I:

The boundary conditions $y(0) = y'(\infty) = 0$ yield:

$$\begin{aligned} l_-(E) &= \lim_{r \rightarrow 0} -\frac{\alpha(E; r)}{\beta(E; r)} \\ l_+(E) &= \lim_{r \rightarrow +\infty} -\frac{\alpha'(E; r)}{\beta'(E; r)} \end{aligned} \quad (89)$$

3. Derivative asymmetric case type II:

The boundary conditions $y'(0) = y(\infty) = 0$ yield:

$$\begin{aligned} l_-(E) &= \lim_{r \rightarrow 0} -\frac{\alpha'(E; r)}{\beta'(E; r)} \\ l_+(E) &= \lim_{r \rightarrow +\infty} -\frac{\alpha(E; r)}{\beta(E; r)} \end{aligned} \quad (90)$$

4. Derivative (Neumann type) boundary conditions:

The boundary conditions $y'(0) = y'(\infty) = 0$ yield:

$$\begin{aligned} l_-(E) &= \lim_{r \rightarrow 0} -\frac{\alpha'(E; r)}{\beta'(E; r)} \\ l_+(E) &= \lim_{r \rightarrow +\infty} -\frac{\alpha'(E; r)}{\beta'(E; r)} \end{aligned} \quad (91)$$

These formulas can also be generalised to arbitrary (Cauchy or mixed type) boundary conditions:

$$\begin{aligned} a_1 y(0) + b_1 y(0) &= c_1 \\ a_2 y(\infty) + b_2 y(\infty) &= c_2 \end{aligned} \quad (92)$$

and to the multichannel case. For instance, in the 1D symmetric Double Gaussian potential the boundary conditions correspond to above case No.3 whereas the asymmetric case corresponds to case No. 2.

References

- [1] M. Aymar, C. H. Green, and E. Luc-Koenig, Rev. Mod. Phys. **68**, 1015 (1996).
- [2] M. Aymar and M. Crance: J. Phys. **B 13**, p. 2527-2544 (1980).
- [3] Bar Shalom A 1983 *PhD. Thesis* University of Jerusalem.
- [4] Bayliss W E and Peel S J 1982 *Comput. Phys. Commun.* **25** 7
- [5] C. Boisseau, E. Audouard, J. Vigué and V. V. Flambaum: Eur. J. Phys. **D12**, 199 (2000).
- [6] C. Boisseau, E. Audouard, J. Vigué: Europhys. Lett. **41**, 349 (1998).
- [7] Bransden B H and Noble C J 1976 *J. Phys. B: At. Mol. Opt. Phys.* **9** 1507.
- [8] Bray I 1994 *Phys. Rev. Lett.* **73** 1088.
- [9] Broyden, CG: Mathematics of Computation, **19**, 557 (1965).
- [10] Burgess A 1963 *Proc. Phys. Soc.* **81** 442.
- [11] A. Crubellier, O. Dulieu, F. Masnou-Seeuws, M. Elbs, H. Knockel and E. Tiemann, Eur. Phys. J. **D6**, 211 (1999).
- [12] Drachman R J and Temkin A 1972 *Case Studies in Atomic Physics* **II**, ed. E W McDaniel and M R C McDowell, North Holland, 399
- [13] Fakhreddine K, Tweed R., Nguyen G., Tannous C., Langlois J. and Robaux O., *Can. J. Phys.* June 2006
- [14] Fakhreddine K and Kobeissi H 1994 *Int. J. Quantum Chem.* **49** 773.
- [15] Fakhreddine K, Kobeissi H and Korec M 1999 *Int. J. Quantum Chem.* **73** 325.
- [16] B. Fornberg, ACM Trans. on Mathematical Software Vol. **7**, No 4, 512 (1981).
- [17] B. Fornberg, ACM Trans. on Mathematical Software Vol. **7**, No 4, 542 (1981).
- [18] R. S. Friedman and M. J. Jamieson: CPC **62**, 53 (1991).
- [19] Furness J B and McCarthy I E 1973 *J. Phys. B: At. Mol. Opt. Phys.* **6** 2280.
- [20] Bo Gao Phys. Rev. Lett. **83**, 4225 (1999).
- [21] A. E. S. Green, D. L. Sellin and A. S. Zachor, Phys. Rev. **184**, 1 (1969).
- [22] I P Hamilton and J C Light: J. Chem. Phys. **84**, 306 (1986).
- [23] Henry R.J. W., Rountree S. P. and Smith E.R. 1981 *Comp. Phys. Comm.* **23** 233.
- [24] H. Hibbert, Adv. At. Mol. Phys. **18** 309 (1982).
- [25] B. R. Johnson: J. Chem. Phys. **67**, 4086 (1977).
- [26] K. M. Jones, P. S. Julianne, P. D. Lett, W. D. Philips, E. Tiesinga and C. J. Williams, Eur. Phys. Lett. **35**, 85 (1996).
- [27] C. Jungen, Molecular Applications of Quantum Defect Theory, Institute of Physics Publishing (1996).
- [28] M. Klapisch, Comp. Phys. Comm. **2**, 239 (1971).
- [29] H. Kobeissi, J. Phys. B **15**, 693 (1982).
- [30] H. Kobeissi and M. Kobeissi, J. Comp. Phys. **77**, 501 (1988).
- [31] H. Kobeissi, K. Fakhreddine and M. Kobeissi, Int. J. Quantum Chemistry, **XL**, 11 (1990).
- [32] Kobeissi H and Fakhreddine K 1991a *J. Phys. II (France)* **1** 899.
- [33] Kobeissi H and Fakhreddine K 1991b *J. Comput. Phys.* **95** 505.
- [34] Kobeissi H Fakhreddine K and Kobeissi M 1991 *Int. J. Quantum Chem.* **XL** 11.
- [35] H. Kobeissi, K. Fakhreddine J. Physique II (France) **1**, 38 (1991).
- [36] R. J. LeRoy and R. B. Bernstein, J. Chem. Phys. **52**, 3869 (1970).
- [37] R. P. McEachran, A. D. Stauffer, J. Phys. **B 16**, 4023 (1983).
- [38] I. E. McCarthy, Aust. J. Phys. **48**, 1 (1995).
- [39] McDowell M R C, Morgan L and Myerscough V P 1974a *Comput. Phys. Commun.* **7** 38.
- [40] McDowell M R C, Myerscough V P and Morgan L 1974b

- J. Phys. B: At. Mol. Opt. Phys.* **24** 657.
- [41] C. E. Moore, Atomic energy levels, NBS Publications (1971).
 - [42] M. Movre and G. Pichler, *J. phys.* **B10**, 2631 (1977).
 - [43] Numerov B 1933 *Obser. Cent. Astrophys. (Russ.)* **2** 188.
 - [44] C. Pan and A. F. Starace, *Phys Rev A* **45**, 4588 (1992).
 - [45] R. K. Peterkop, *Theory of Ionization of Atoms By Electron Impact* (Colorado Associated University Press, Boulder) (1977).
 - [46] A. D. Raptis and J.R. Cash: *CPC* **36**, p. 113-119 (1985).
 - [47] A. D. Raptis and J.R. Cash: *CPC* **44**, p. 95-103 (1987).
 - [48] A. R. P. Rau and M. Inokuti: *Am. J. Physics*, **65**, p. 221-225 (1997).
 - [49] Rawitscher G.H, Kang S-Y and Koltracht I. 2003 *J. Chem. Phys.* **118** 9149.
 - [50] Numerical Recipes in C: The Art of Scientific Computing, W. H. Press, W. T. Vetterling, S. A. Teukolsky and B. P. Flannery, Second Edition, page 389, Cambridge University Press (New-York, 1992).
 - [51] M.E. Riley and D.G. Trular, *J. Chem. Phys.* **63**, 2182 (1975).
 - [52] P.J.P. Roche, S. Kawano, C.T. Whelan, J. Rasch, H. R. J. Walters, R. J. Allan, J. Langlois and C. Tannous 2001, Chapter 7, pp. 81-90, in *Many-Particle Spectroscopy of Atoms, Molecules, Clusters and Surfaces* edited by J. Berakdar and J. Kirschner, Kluwer Academic/Plenum Publishers (New-York, 2001).
 - [53] C. Jungen, A.L. Roche, M Arif, *Phil. Trans. A* **355**, 2520 (1997).
 - [54] Rouet F, Tweed R J and Langlois J J. *Phys. B: At. Mol. Opt. Phys.* **29** 1767 (1996).
 - [55] B. Rouvellou, S. Rioual, J. Roeder, A. Pochat, J. Rasch, C. T. Whelan, H. R. J. Walters and R. J. Allan, *Phys. Rev. A* **57**, 3621 (1998).
 - [56] Scott T and McDowell M R C 1975 *J. Phys. B: At. Mol. Opt. Phys.* **8** 1851.
 - [57] W.C. Stwalley, Y.H. Uang and G. Pichler, *Phys. Rev. Lett.* **41**, 1165 (1978).
 - [58] P. P. Szydlik and A. E. S.Green, *Phys. Rev. A* **9**, 1885 (1974).
 - [59] C. Tannous, K. Fakhreddine and J. Langlois, *J. Phys. IV France* **9** Pr6-71 (1999).
 - [60] J. Trost, C. Eltschka and H. Friedrich: *J. Phys.* **B31**, 361 (1998).
 - [61] I. E. McCarthy and E. Weigold, *Electron-atom collisions*, Cambridge University Press (1995).
 - [62] Whelan C. T. 1999 in *New Directions in Atomic Physics*, edited by C.T. Whelan, R. M. Dreizler, J. H. Macek and H. R. J. Walters (Kluwer/Plenum, New York).
 - [63] K. D. Winkler, D. H. Madison and H. P. Saha *J. Phys. B* **32**, 1987 (1999).